Supplementary Information

The microscopic origin of a hesitant world: Quadrangular holes govern path multiplicity in complex networks

Ye Deng[1,2], Jun Wu[1,2,*], Xin Lu[3*], Petter Holme[4,5*], Daqing Li[6,7*], Zengru Di[1,2,8], Guanrong Chen[9], Jürgen Kurths[10,11]

[1]Department of Systems Science, Faculty of Arts and Sciences, Beijing Normal University, Zhuhai 519087, China; [2]International Academic Center of Complex Systems, Beijing Normal University, Zhuhai 519087, China; [3]College of Systems Engineering, National University of Defense Technology, Changsha 410073, China; [4]Department of Computer Science, Aalto University, Espoo 02150, Finland; [5]Center for Computational Social Science, Kobe University, Kobe 657-8501, Japan; [6]School of Reliability and Systems Engineering, Beihang University, Beijing 100083, China; [7]Department of Science and Technology, Civil Aviation University of China, Tianjin 300300, China; [8]School of Systems Science, Beijing Normal University, Beijing 100875, China; [9]Department of Electrical Engineering, City University of Hong Kong, Hong Kong SAR, China; [10]Research Domain Complexity Science, Potsdam Institute for Climate Impact Research, Potsdam 14473, Germany; [11]Department of Physics, Humboldt-Universität zu Berlin, Berlin 12489, Germany

This PDF file includes:

Table S1. Metadata of 140 real-world networks, where N is the number of nodes, n_c is the number of communities, $\langle k \rangle$ is the average degree, L is the average shortest path length, E_{glob} is the global efficiency, D is the diameter, r is the assortativity coefficient, C is the clustering coefficient, k_s is the maximum k-core, $|\mathcal{H}_3(G)|$ is the number of triangles, $|\mathcal{H}_4(G)|$ is the number of chordless 4-cycles, $|\mathcal{H}_5(G)|$ is the number of chordless 5-cycles, and $|\mathcal{H}_6(G)|$ is the number of chordless 6-cycles. For each real network, we analyze the largest connected component to avoid artifacts from disconnected components.

No.	*Name*	*RPMI*	*PMI*	n_c	$\langle k \rangle$	L	E_{glob}	D	r	C	k_s	$\lvert\mathcal{H}_3(G)\rvert$	$\lvert\mathcal{H}_4(G)\rvert$	$\lvert\mathcal{H}_5(G)\rvert$	$\lvert\mathcal{H}_6(G)\rvert$
1	bn-cat-mixed-species-brain-1	1.08	5.76	3	22.46	1.70	0.67	3	-0.03	0.66	16	3613	4568	5077	5101
2	bn-macaque-rhesus-brain-2	0.98	4.04	2	12.79	1.87	0.57	3	-0.77	0.86	11	1902	1649	87	0
3	bn-macaque-rhesus-cerebral-cortex-1	1.12	8.07	3	30.79	1.66	0.67	3	-0.55	0.74	22	10336	16425	10777	10522
4	bn-macaque-rhesus-interareal-cortical-network-2	1.13	14.20	1	48.65	1.47	0.76	2	-0.70	0.85	29	29638	0	0	0
5	bn-mouse-kasthuri-graph-v4	7.91	13.20	21	3.11	4.91	0.23	12	-0.24	0	3	0	770	0	11547
6	bn-mouse-brain-1	0.89	27.96	2	151.07	1.29	0.86	2	-0.07	0.76	111	622414	3051871	9377953	16227275
7	bn-mouse-retina-1	1.31	29.49	4	168.79	1.86	0.58	4	-0.20	0.59	121	3289057	47425907	1286844748	31237454889
8	bn-mouse-visual-cortex-1-2	1.48	2.11	3	3.03	2.94	0.42	6	-0.47	0.05	2	1	13	5	27
9	aves-barn-swallow-contact-network	0.99	2.08	2	6.24	1.73	0.68	4	-0.31	0.55	5	55	51	1	3
10	aves-barn-swallow-non-physical	0.85	1.85	2	14.35	1.10	0.95	2	-0.15	0.93	13	510	3	0	0
11	aves-sparrow-social	1.14	4.79	4	17.46	1.75	0.66	3	-0.06	0.72	13	1857	906	1013	1231
12	aves-sparrow-social-2009	0.90	3.24	3	13.61	1.89	0.68	4	0.29	0.77	12	721	397	215	26
13	aves-sparrow-social-2010	0.98	3.96	4	15.25	1.65	0.69	3	-0.12	0.71	11	1045	449	503	393
14	aves-sparrowlyon-flock-season2	0.99	2.58	3	6.98	2.02	0.55	3	-0.63	0.67	8	248	81	0	0

Continued on next page

No.	*Name*	$RPMI$	PMI	n_c	$\langle k \rangle$	L	E_{glob}	D	r	C	k_s	$\lvert\mathcal{H}_3(G)\rvert$	$\lvert\mathcal{H}_4(G)\rvert$	$\lvert\mathcal{H}_5(G)\rvert$	$\lvert\mathcal{H}_6(G)\rvert$
15	aves-sparrowlyon-flock-season3	1.03	3.44	2	12.07	1.61	0.72	3	0.07	0.74	10	472	42	121	84
16	aves-thornbill-farine	0.94	3.23	3	10.16	1.85	0.58	3	-0.75	0.87	8	751	415	0	0
17	bio-CE-GT	2.53	7.72	22	7.25	3.73	0.30	10	-0.19	0.59	9	3959	11705	16844	80438
18	bio-CE-LC	3.50	4.79	91	2.62	7.92	0.15	22	-0.26	0.08	4	148	471	35	357
19	bio-CE-PG	0.60	1.58	3	5.67	2.09	0.49	3	-0.55	0.49	9	4410	0	0	0
20	bio-DM-HT	6.30	10.85	243	3.22	8.14	0.13	19	-0.10	0.01	11	118	12683	41	122
21	bio-DM-LC	21.20	44.67	34	4.13	6.61	0.19	18	-0.19	0.12	10	194	9642	142	5717
22	bio-DR-CX	1.49	27.72	4	51.68	2.78	0.39	7	0.34	0.20	95	1026290	12091300	434866528	10500747650
23	bio-HS-HT	3.47	13.72	50	10.92	4.06	0.27	12	0.29	0.17	39	48888	194960	625794	6824137
24	bio-SC-LC	4.32	21.50	15	20.46	3.24	0.33	7	0.19	0.17	48	75957	1375383	4990829	97394501
25	bio-SC-TS	1.05	4.52	2	12.93	1.88	0.56	3	-0.88	0.90	9	2144	0	0	0
26	bio-celegans	1.37	4.92	8	8.94	2.66	0.41	7	-0.23	0.65	10	3284	4493	11720	45296
27	bio-celegans-dir	1.37	4.92	8	8.94	2.66	0.41	7	-0.23	0.65	10	3284	4493	11720	45296
28	bio-grid-mouse	6.65	9.78	66	2.78	8.66	0.15	30	-0.21	0.05	6	105	3099	23	17328
29	bio-grid-plant	3.77	8.22	137	4.29	8.29	0.15	26	0.00	0.17	12	2477	7149	2787	4914
30	bio-grid-worm	3.27	6.58	36	3.85	4.32	0.25	13	-0.17	0.05	10	2090	32679	42919	406191
31	bio-yeast	1.83	2.58	152	2.67	6.81	0.16	19	-0.21	0.07	5	206	139	113	258
32	bio-yeast-protein-inter	1.84	2.58	152	2.67	6.81	0.16	19	-0.21	0.07	5	206	139	113	258
33	ca-AstroPh	3.43	25.18	611	22.00	4.19	0.26	14	0.20	0.63	56	1350014	1302079	33997621	1054735601
34	ca-CSphd	1.58	1.53	138	2.04	11.75	0.11	28	-0.25	0.00	2	4	5	0	1
35	ca-CondMat	3.37	11.84	979	8.55	5.35	0.20	15	0.13	0.64	25	171051	37757	365462	4458410
36	ca-Erdos992	2.87	4.56	430	2.98	5.51	0.19	14	-0.45	0.08	7	1610	1895	5914	27224
37	ca-GrQc	1.87	5.40	494	6.46	6.05	0.18	17	0.64	0.56	43	47779	1115	3358	12502
38	ca-HepPh	2.81	21.83	206	21.00	4.67	0.23	13	0.63	0.62	238	3357890	820741	13431707	218007076
39	eco-everglades	1.14	7.03	3	25.51	1.64	0.69	3	-0.30	0.55	20	4348	20426	8985	10443
40	eco-foodweb-baydry	1.43	9.37	4	32.91	1.77	0.62	3	-0.10	0.33	24	8715	139200	366032	1753157
41	eco-foodweb-baywet	1.41	9.17	4	32.42	1.78	0.62	3	-0.11	0.33	23	8437	131661	350309	1686287
42	eco-mangwet	1.07	7.07	3	29.81	1.69	0.65	3	-0.15	0.47	23	7494	58777	69466	159659

Continued on next page

No.	*Name*	*RPMI*	*PMI*	n_c	$\langle k \rangle$	L	E_{glob}	D	r	C	k_s	$\lvert\mathcal{H}_3(G)\rvert$	$\lvert\mathcal{H}_4(G)\rvert$	$\lvert\mathcal{H}_5(G)\rvert$	$\lvert\mathcal{H}_6(G)\rvert$
43	eco-stmarks	0.91	3.12	4	12.96	1.76	0.62	3	-0.23	0.41	10	650	2542	2844	4776
44	ENZYMES-g118	1.80	2.27	11	2.55	7.57	0.19	18	0.10	0	2	0	12	2	8
45	ENZYMES-g196	1.06	1.83	6	3.44	4.12	0.32	10	-0.06	0.21	3	17	10	5	10
46	ENZYMES-g198	1.15	1.65	6	2.80	5.15	0.27	13	0.06	0.19	2	9	5	3	8
47	ENZYMES-g203	1.31	2.33	5	3.57	4.74	0.29	11	0.22	0.28	3	31	19	6	3
48	ENZYMES-g209	1.35	2.29	6	3.54	4.80	0.29	11	0.23	0.28	3	31	19	3	5
49	ENZYMES-g349	1.49	2.64	7	3.69	5.35	0.28	12	-0.23	0.24	3	26	20	20	34
50	ENZYMES-g465	1.43	2.62	7	3.81	4.43	0.31	9	0.01	0.25	3	23	22	17	15
51	ENZYMES-g484	1.48	2.02	5	2.67	6.01	0.24	13	0.06	0.15	2	7	7	3	3
52	ENZYMES-g501	1.45	1.67	8	2.42	7.14	0.21	18	0.49	0.01	3	2	20	2	13
53	ENZYMES-g532	1.47	2.27	7	3.24	4.75	0.28	12	0.20	0.09	3	16	29	19	8
54	ENZYMES-g541	1.40	1.78	6	2.64	3.80	0.35	8	-0.07	0.06	2	2	8	0	1
55	econ-mahindas	6.53	30.46	10	11.94	3.57	0.31	8	-0.06	0.06	40	3414	1339064	61294	4128399
56	econ-poli	4.28	4.85	216	2.28	10.20	0.12	27	-0.34	0.07	5	173	325	50	26
57	econ-wm3	1.58	10.22	5	18.51	2.61	0.44	6	-0.06	0.27	33	21697	30164	21562	107057
58	ia-email-univ	1.75	6.74	14	9.62	3.61	0.30	8	0.08	0.22	11	5343	12628	76309	598387
59	ia-hospital-ward-proximity	0.96	7.33	3	30.37	1.60	0.70	3	-0.18	0.64	22	8215	12668	18992	23780
60	ia-hospital-ward-proximity-attr	0.96	7.33	3	30.37	1.60	0.70	3	-0.18	0.64	22	8215	12668	18992	23780
61	ia-infect-hyper	0.95	8.69	4	38.87	1.66	0.67	3	-0.12	0.53	28	16867	69350	278748	898126
62	ia-reality	4.44	5.06	337	2.26	4.21	0.25	8	-0.68	0.02	5	400	2770	4082	45531
63	ia-southernwomen	0.87	1.96	2	7.11	1.62	0.70	3	-0.36	0.76	6	97	25	0	0
64	ia-workplace-contacts	1.28	5.05	4	16.41	1.96	0.57	3	-0.06	0.43	11	1752	3997	17575	74522
65	power-1138-bus	2.18	2.94	56	2.56	12.72	0.10	31	-0.08	0.09	4	128	78	53	51
66	power-494-bus	1.89	2.29	29	2.37	10.47	0.12	26	-0.07	0.04	2	21	21	10	6
67	power-662-bus	1.69	2.45	27	2.74	10.24	0.12	25	-0.07	0.05	4	59	55	35	39
68	power-685-bus	3.73	7.29	17	3.74	12.42	0.11	26	0.18	0.17	5	330	192	207	223
69	power-US-Grid	5.00	6.99	141	2.67	18.99	0.06	46	0.00	0.08	5	651	324	311	331

Continued on next page

No.	*Name*	*RPMI*	*PMI*	n_c	$\langle k \rangle$	L	E_{glob}	D	r	C	k_s	$\lvert\mathcal{H}_3(G)\rvert$	$\lvert\mathcal{H}_4(G)\rvert$	$\lvert\mathcal{H}_5(G)\rvert$	$\lvert\mathcal{H}_6(G)\rvert$
70	power-bcspwr09	3.10	4.57	76	2.78	15.49	0.08	37	-0.10	0.08	3	174	159	191	202
71	power-bcspwr10	3.90	6.54	100	3.12	20.85	0.06	49	-0.05	0.09	4	721	700	657	856
72	copresence-InVS13	0.66	6.28	2	82.42	1.12	0.94	2	-0.03	0.93	78	101236	13423	4047	453
73	hospital-ward-proximity	0.96	7.33	3	30.37	1.60	0.70	3	-0.18	0.64	22	8215	12668	18992	23780
74	infect-hyper	0.96	8.69	4	38.87	1.66	0.67	3	-0.12	0.53	28	16867	69350	278748	898126
75	primary-school-proximity	1.10	15.69	4	68.74	1.73	0.64	3	0.12	0.53	47	103760	760419	8321360	79399826
76	road-City-of-Oldenburg	2.15	2.49	120	2.30	40.69	0.03	104	0.06	0.01	2	41	124	72	101
77	road-beijing	12.79	18.61	101	2.73	36.92	0.03	89	0.27	0.02	2	153	780	187	154
78	road-chesapeake	0.94	2.72	3	8.72	1.84	0.60	3	-0.38	0.45	6	194	839	228	116
79	road-euroroad	2.33	3.04	25	2.51	18.40	0.08	62	0.09	0.02	2	32	38	52	43
80	road-minnesota	7.30	9.57	40	2.50	35.35	0.04	99	-0.19	0.02	2	53	54	47	52
81	tech-routers-rf	2.39	6.78	135	6.28	4.61	0.24	12	0.02	0.25	15	10404	22816	22762	142077
82	email-dnc	2.58	6.09	18	4.76	3.37	0.32	8	-0.31	0.22	17	9431	16208	43358	153478
83	email-univ	1.77	6.74	14	9.62	3.61	0.30	8	0.08	0.22	11	5343	12628	76309	598387
84	inf-USAir97	1.31	5.58	4	12.81	2.74	0.41	6	-0.21	0.63	26	12181	4533	4110	5048
85	inf-euroroad	2.37	3.04	25	2.51	18.40	0.08	62	0.09	0.02	2	32	38	52	43
86	inf-openflights	5.65	21.82	29	10.77	4.10	0.27	14	0.05	0.46	28	72843	319407	1632910	11884654
87	inf-power	5.00	6.99	141	2.67	18.99	0.06	46	0.00	0.08	5	651	324	311	331
88	london-overground	1.52	1.78	21	2.33	13.73	0.10	39	0.14	0.03	2	13	12	4	9
89	london-underground	1.52	1.75	19	2.30	13.96	0.10	39	0.14	0.03	2	10	11	3	8
90	web-EPA	3.71	7.96	113	4.18	4.50	0.24	10	-0.30	0.07	6	997	20160	20991	263470
91	web-indochina-2004	8.42	28.55	1105	8.38	6.42	0.18	27	0.12	0.71	49	210078	9187	503	482
92	web-spam	3.22	18.82	28	15.68	3.79	0.29	12	0.00	0.29	35	129017	1458084	18521029	320394705
93	web-webbase-2001	35.76	60.96	1327	3.19	10.21	0.12	23	-0.10	0.22	32	21115	20420	8545	27865
94	soc-dolphins	1.36	3.00	4	5.13	3.36	0.38	8	-0.04	0.26	4	95	59	142	239
95	soc-firm-hi-tech	0.99	2.23	3	5.52	2.36	0.51	5	-0.09	0.45	5	77	35	69	42
96	soc-hamsterster	5.43	30.00	28	16.10	3.59	0.31	10	0.02	0.54	24	52651	200462	2623585	36156328
97	soc-karate	1.40	2.77	4	4.59	2.41	0.49	5	-0.48	0.57	4	45	36	20	2
98	soc-tribes	0.93	2.18	3	7.25	1.54	0.74	3	0.05	0.54	5	68	56	47	17
99	soc-wiki-Vote	2.42	7.06	12	6.56	4.10	0.27	13	-0.03	0.15	9	2119	6873	25010	104736

Continued on next page

No.	*Name*	*RPMI*	*PMI*	n_c	$\langle k \rangle$	L	E_{glob}	D	r	C	k_s	$\|\mathcal{H}_3(G)\|$	$\|\mathcal{H}_4(G)\|$	$\|\mathcal{H}_5(G)\|$	$\|\mathcal{H}_6(G)\|$
100	fb-pages-food	3.08	9.00	62	6.75	5.09	0.24	17	-0.03	0.33	11	2935	9003	12403	42583
101	fb-pages-politician	4.09	19.00	205	14.12	4.66	0.23	14	0.02	0.39	31	174632	630811	2110870	11564939
102	fb-pages-public-figure	5.58	25.44	295	11.59	4.62	0.23	15	0.20	0.18	42	184838	3384130	45669068	870671995
103	fb-pages-tvshow	4.98	18.28	508	8.86	6.28	0.18	20	0.56	0.37	56	87090	35915	31987	139241
104	socfb-Reed98	1.30	16.60	4	39.11	2.46	0.44	6	0.02	0.32	34	97137	1237142	26933744	562139763
105	socfb-nips-ego	1.58	1.53	17	2.06	3.87	0.29	9	-0.67	0.03	3	91	15	2	16
106	rt-retweet	1.32	1.53	10	2.44	4.31	0.28	10	-0.18	0.06	3	12	14	3	4
107	rt-twitter-copen	1.84	2.63	42	2.70	5.35	0.21	14	-0.10	0.08	4	149	183	349	697
108	rt-assad	3.42	4.68	50	2.61	5.21	0.21	14	-0.26	0.01	5	220	1629	4035	20053
109	rt-damascus	4.61	6.09	399	2.54	5.12	0.22	13	-0.16	0.01	5	165	1502	2542	17353
110	rt-obama	5.58	5.70	254	2.13	7.31	0.16	18	-0.28	0.00	3	14	199	60	656
111	rt-occupy	3.22	4.11	268	2.44	5.72	0.20	24	-0.14	0.01	4	115	725	1854	9776
112	rt-voteonedirection	12.54	13.14	66	2.16	4.75	0.25	16	-0.39	0.00	3	3	1899	12	26214
113	C125-9	1.00	10.94	2	111.41	1.10	0.95	2	-0.02	0.90	102	230619	191408	18995	204
114	MANN-a9	1.05	3.76	1	40.80	1.07	0.96	2	0.00	0.92	40	11244	2106	0	0
115	brock200-1	1.00	28.78	3	148.34	1.25	0.87	2	-0.00	0.75	134	543700	3900964	7471673	3734928
116	gen200-p0-9-44	0.99	16.90	2	179.10	1.10	0.95	2	-0.01	0.90	167	958030	1257669	177670	3788
117	johnson8-4-4	1.09	10.97	5	53	1.23	0.88	2	0	0.74	53	23940	73360	4032	3360
118	san200-0-9-1	0.98	16.62	2	179.10	1.10	0.95	2	0.04	0.90	162	960241	1215190	141944	822
119	bio-celegansneural	1.41	7.14	4	14.46	2.46	0.44	5	-0.16	0.29	10	3241	15863	88393	625342
120	chesapeake	0.93	2.72	3	8.72	1.84	0.60	3	-0.38	0.45	6	194	839	228	116
121	delaunay-n10	23.12	63.33	14	5.97	10.32	0.12	20	-0.12	0.44	4	2047	114	372	729
122	delaunay-n11	63.59	174.70	18	5.98	13.35	0.09	26	-0.10	0.44	4	4104	270	763	1414
123	insecta-ant-trophallaxis-colony1	1.05	3.47	3	12.49	1.74	0.65	3	0.00	0.39	9	445	1167	2807	4475
124	insecta-ant-trophallaxis-colony2	1.07	3.49	2	12.56	1.76	0.65	4	-0.15	0.42	10	501	1114	2342	2868
125	mammalia-raccoon-proximity	0.73	2.53	2	18.83	1.18	0.91	2	-0.13	0.90	17	1252	24	0	0
126	reptilia-tortoise-network-bsv	1.32	3.25	9	5.54	3.46	0.34	9	0.20	0.37	6	293	157	313	437

Continued on next page

No.	*Name*	$RPMI$	PMI	n_c	$\langle k \rangle$	L	E_{glob}	D	r	C	k_s	$\lvert\mathcal{H}_3(G)\rvert$	$\lvert\mathcal{H}_4(G)\rvert$	$\lvert\mathcal{H}_5(G)\rvert$	$\lvert\mathcal{H}_6(G)\rvert$
127	reptilia-tortoise-network-cs	1.10	2.60	5	6	2.40	0.52	6	-0.00	0.46	5	96	63	44	32
128	reptilia-tortoise-network-fi	1.80	3.62	54	3.97	7.93	0.16	21	0.35	0.34	8	743	104	166	321
129	reptilia-tortoise-network-hw	1.48	1.27	2	2	1.73	0.68	3	-0.73	0	2	0	1	0	0
130	reptilia-tortoise-network-lm	1.10	2.21	4	4.88	2.64	0.45	6	0.04	0.38	5	78	47	46	38
131	reptilia-tortoise-network-pv	1.07	2.06	3	4.45	2.46	0.52	6	-0.18	0.52	5	51	0	0	0
132	DD199	62.58	141.27	36	4.52	16.09	0.09	59	0.33	0.47	4	1186	126	43	52
133	DD68	7.95	20.52	24	5.40	12.12	0.13	41	0.43	0.44	5	1472	333	261	551
134	DD687	4.70	14.32	16	7.17	6.45	0.18	17	0.36	0.47	5	2523	485	733	1726
135	citeseer	3.51	6.47	165	3.48	9.31	0.13	28	0.01	0.17	7	1083	3058	3150	7511
136	cora	2.42	5.07	149	4.08	6.31	0.18	19	-0.07	0.24	4	1558	1523	1840	4752
137	gene	1.70	3.16	67	3.53	7.01	0.17	22	0.14	0.22	12	809	180	92	135
138	internet-industry-partnerships	1.35	3.51	6	5.75	2.98	0.37	6	-0.22	0.18	6	328	1434	3950	11671
139	webkb-wisc	2.11	3.87	13	3.59	3.26	0.35	8	-0.19	0.21	4	118	359	95	69
140	tech-WHOIS	3.56	17.37	102	15.23	3.54	0.30	8	-0.04	0.49	88	782494	2934453	31835788	397659584

16

Table S2. Metadata of 140 real-world networks, where N is the number of nodes, n_c is the number of communities, $\langle k \rangle$ is the average degree, L is the average shortest path length, E_{glob} is the global efficiency, D is the diameter, r is the assortativity coefficient, C is the clustering coefficient, k_s is the maximum k-core, $|\mathcal{H}_3(G)|$ is the number of triangles, $|\mathcal{H}_4(G)|$ is the number of chordless 4-cycles, $|\mathcal{H}_5(G)|$ is the number of chordless 5-cycles, $|\mathcal{H}_6(G)|$ is the number of chordless 6-cycles, $\tilde{\mathcal{H}}_3(G)$ is the density of triangles, $\tilde{\mathcal{H}}_4(G)$ is the density of chordless 4-cycles, $\tilde{\mathcal{H}}_5(G)$ is the density of chordless 5-cycles, and $\tilde{\mathcal{H}}_6(G)$ is the density of chordless 6-cycles. For each real network, we analyze the largest connected component to avoid artifacts from disconnected components.

No.	*Name*	*RPMI*	*PMI*	*N*	$\lvert\mathcal{H}_3(G)\rvert$	$\lvert\mathcal{H}_4(G)\rvert$	$\lvert\mathcal{H}_5(G)\rvert$	$\lvert\mathcal{H}_6(G)\rvert$	$\tilde{\mathcal{H}}_3(G)$	$\tilde{\mathcal{H}}_4(G)$	$\tilde{\mathcal{H}}_5(G)$	$\tilde{\mathcal{H}}_6(G)$
1	bn-cat-mixed-species-brain-1	1.0756	5.7591	65	3613	4568	5077	5101	1.9134	0.3519	0.0835	0.0269
2	bn-macaque-rhesus-brain-2	0.9842	4.0379	91	1902	1649	87	0	5.4536	0.6849	0.0058	0.0000
3	bn-macaque-rhesus-cerebral-cortex-1	1.1219	8.0681	91	10336	16425	10777	10522	2.1246	0.3455	0.0334	0.0071
4	bn-macaque-rhesus-interareal-cortical-network-2	1.1343	14.1950	93	29638	0	0	0	1.5450	0.0000	0.0000	0.0000
5	bn-mouse-kasthuri-graph-v4	7.9077	13.2047	987	0	770	0	11547	0.0000	66.1901	0.0000	158.2541
6	bn-mouse-brain-1	0.8874	27.9580	213	622414	3051871	9377953	16227275	1.0832	0.5729	0.6224	1.2779
7	bn-mouse-retina-1	1.3096	29.4874	1076	3289057	47425907	1286844748	31237454889	4.1035	0.6590	0.2217	0.0760
8	bn-mouse-visual-cortex-1-2	1.4822	2.1108	29	1	13	5	27	0.2150	1.6637	0.4165	1.6417
9	aves-barn-swallow-contact-network	0.9912	2.0809	17	55	51	1	3	1.3666	0.8315	0.0177	0.0982
10	aves-barn-swallow-non-physical	0.8488	1.8529	17	510	3	0	0	1.0390	0.0612	0.0000	0.0000
11	aves-sparrow-social	1.1362	4.7888	52	1857	906	1013	1231	2.0935	0.1877	0.0561	0.0272
12	aves-sparrow-social-2009	0.9034	3.2409	31	721	397	215	26	1.7168	0.3325	0.1127	0.0156
13	aves-sparrow-social-2010	0.9755	3.9551	40	1045	449	503	393	1.7691	0.1889	0.0832	0.0414
14	aves-sparrowlyon-flock-season2	0.9929	2.5770	43	248	81	0	0	4.3842	0.4132	0.0000	0.0000

Continued on next page

No.	*Name*	*RPMI*	*PMI*	*N*	$\lvert\mathcal{H}_3(G)\rvert$	$\lvert\mathcal{H}_4(G)\rvert$	$\lvert\mathcal{H}_5(G)\rvert$	$\lvert\mathcal{H}_6(G)\rvert$	$\tilde{\mathcal{H}}_3(G)$	$\tilde{\mathcal{H}}_4(G)$	$\tilde{\mathcal{H}}_5(G)$	$\tilde{\mathcal{H}}_6(G)$
15	aves-sparrowlyon-flock-season3	1.0288	3.4387	27	472	42	121	84	1.6113	0.0598	0.1312	0.1300
16	aves-thornbill-farine	0.9397	3.2263	63	751	415	0	0	4.2992	0.4609	0.0000	0.0000
17	bio-CE-GT	2.5329	7.7224	878	3959	11705	16844	80438	62.4367	34.6149	8.8399	7.2601
18	bio-CE-LC	3.4967	4.7938	993	148	471	35	357	49.4699	80.7583	2.8965	13.7399
19	bio-CE-PG	0.6010	1.5815	734	4410	0	0	0	145.3446	0.0000	0.0000	0.0000
20	bio-DM-HT	6.3013	10.8539	2831	118	12683	41	122	21.1494	943.2514	1.1880	1.3241
21	bio-DM-LC	21.2030	44.6744	483	194	9642	142	5717	16.5433	271.2841	1.2491	15.2560
22	bio-DR-CX	1.4943	27.7228	3287	1026290	12091300	434866528	10500747650	44.6076	14.0038	12.7866	7.6477
23	bio-HS-HT	3.4721	13.7214	2499	48888	194960	625794	6824137	224.9907	110.5618	41.1943	50.2977
24	bio-SC-LC	4.3169	21.5007	1999	75957	1375383	4990829	97394501	53.2249	64.1824	14.6984	17.5668
25	bio-SC-TS	1.0518	4.5234	101	2144	0	0	0	5.9505	0.0000	0.0000	0.0000
26	bio-celegans	1.3685	4.9195	453	3284	4493	11720	45296	27.5731	5.8814	2.2927	1.2998
27	bio-celegans-dir	1.3694	4.9195	453	3284	4493	11720	45296	27.5731	5.8814	2.2927	1.2998
28	bio-grid-mouse	6.6541	9.7835	791	105	3099	23	17328	29.4424	421.3541	1.4284	474.1467
29	bio-grid-plant	3.7729	8.2150	1272	2477	7149	2787	4914	188.7431	170.8749	19.6716	9.8738
30	bio-grid-worm	3.2690	6.5846	3343	2090	32679	42919	406191	219.5663	1192.0956	510.4073	1513.9955
31	bio-yeast	1.8313	2.5769	1458	206	139	113	258	64.7790	21.9205	8.3994	8.6995
32	bio-yeast-protein-inter	1.8357	2.5769	1458	206	139	113	258	64.7790	21.9205	8.3994	8.6995
33	ca-AstroPh	3.4334	25.1806	17903	1350014	1302079	33997621	1054735601	760.2630	44.5461	66.3281	112.7974
34	ca-CSphd	1.5825	1.5309	1025	4	5	0	1	2.8473	2.3457	0.0000	0.1735
35	ca-CondMat	3.3680	11.8434	21363	171051	37757	365462	4458410	1644.2182	56.6743	80.3434	137.8712
36	ca-Erdos992	2.8702	4.5561	4991	1610	1895	5914	27224	366.2969	193.4341	254.1202	473.1090
37	ca-GrQc	1.8685	5.4007	4158	47779	1115	3358	12502	1065.3697	5.1532	3.0211	2.1057
38	ca-HepPh	2.8059	21.8267	11204	3357890	820741	13431707	218007076	2176.7817	33.9208	33.2451	31.0833
39	eco-everglades	1.1377	7.0286	69	4348	20426	8985	10443	1.5723	1.0187	0.0942	0.0359
40	eco-foodweb-baydry	1.4322	9.3675	128	8715	139200	366032	1753157	1.4676	1.7580	0.4422	0.2647
41	eco-foodweb-baywet	1.4071	9.1694	128	8437	131661	350309	1686287	1.4854	1.7464	0.4443	0.2657
42	eco-mangwet	1.0693	7.0692	97	7494	58777	69466	159659	1.6968	1.2788	0.1996	0.0853

Continued on next page

No.	*Name*	*RPMI*	*PMI*	*N*	$\lvert\mathcal{H}_3(G)\rvert$	$\lvert\mathcal{H}_4(G)\rvert$	$\lvert\mathcal{H}_5(G)\rvert$	$\lvert\mathcal{H}_6(G)\rvert$	$\tilde{\mathcal{H}}_3(G)$	$\tilde{\mathcal{H}}_4(G)$	$\tilde{\mathcal{H}}_5(G)$	$\tilde{\mathcal{H}}_6(G)$
43	eco-stmarks	0.9088	3.1181	54	650	2542	2844	4776	1.7910	1.3120	0.3481	0.1797
44	ENZYMES-g118	1.7952	2.2674	95	0	12	2	8	0.0000	2.4613	0.2258	0.4960
45	ENZYMES-g196	1.0641	1.8327	50	17	10	5	10	2.5067	0.6892	0.1659	0.1687
46	ENZYMES-g198	1.1528	1.6505	55	9	5	3	8	2.4608	0.7520	0.2502	0.3821
47	ENZYMES-g203	1.3057	2.3312	56	31	19	6	3	4.0844	1.1092	0.1586	0.0376
48	ENZYMES-g209	1.3509	2.2888	57	31	19	3	5	4.1804	1.1393	0.0816	0.0644
49	ENZYMES-g349	1.4856	2.6394	64	26	20	20	34	3.1120	1.0086	0.4302	0.3235
50	ENZYMES-g465	1.4310	2.6237	52	23	22	17	15	2.5007	1.0181	0.3463	0.1425
51	ENZYMES-g484	1.4834	2.0243	60	7	7	3	3	2.2155	1.2577	0.3058	0.1776
52	ENZYMES-g501	1.4527	1.6732	66	2	20	2	13	0.8425	5.1583	0.3125	1.2474
53	ENZYMES-g532	1.4661	2.2658	74	16	29	19	8	2.8146	2.3615	0.7127	0.1409
54	ENZYMES-g541	1.4041	1.7804	28	2	8	0	1	0.6510	1.7433	0.0000	0.1271
55	econ-mahindas	6.5349	30.4553	1258	3414	1339064	61294	4128399	12.0206	537.3104	2.6550	18.7249
56	econ-poli	4.2807	4.8481	2343	173	325	50	26	87.9741	97.0657	8.2339	2.2696
57	econ-wm3	1.5775	10.2173	257	21697	30164	21562	107057	20.5156	2.4056	0.1472	0.0650
58	ia-email-univ	1.7528	6.7378	1133	5343	12628	76309	598387	35.9839	12.0089	9.6973	9.8476
59	ia-hospital-ward-proximity	0.9573	7.3337	75	8215	12668	18992	23780	1.7594	0.3522	0.1105	0.0478
60	ia-hospital-ward-proximity-attr	0.9561	7.3337	75	8215	12668	18992	23780	1.7594	0.3522	0.1105	0.0478
61	ia-infect-hyper	0.9514	8.6923	113	16867	69350	278748	898126	1.7237	0.5806	0.2770	0.1572
62	ia-reality	4.4410	5.0597	6809	400	2770	4082	45531	209.0681	856.5523	700.4425	4164.0033
63	ia-southernwomen	0.8721	1.9608	18	97	25	0	0	1.6241	0.2629	0.0000	0.0000
64	ia-workplace-contacts	1.2810	5.0535	92	1752	3997	17575	74522	2.3778	0.6707	0.4218	0.3031
65	power-1138-bus	2.1787	2.9435	1138	128	78	53	51	45.6484	14.5656	4.8737	2.2240
66	power-494-bus	1.8915	2.2946	494	21	21	10	6	9.4356	5.3761	1.3769	0.4295
67	power-662-bus	1.6901	2.4478	662	59	55	35	39	17.2625	7.9282	2.3435	1.1711
68	power-685-bus	3.7258	7.2922	685	330	192	207	223	37.7558	7.9345	2.9170	1.0359
69	power-US-Grid	4.9971	6.9937	4941	651	324	311	331	205.4184	51.1473	23.0437	11.0593

Continued on next page

No.	*Name*	*RPMI*	*PMI*	*N*	$\lvert\mathcal{H}_3(G)\rvert$	$\lvert\mathcal{H}_4(G)\rvert$	$\lvert\mathcal{H}_5(G)\rvert$	$\lvert\mathcal{H}_6(G)\rvert$	$\tilde{\mathcal{H}}_3(G)$	$\tilde{\mathcal{H}}_4(G)$	$\tilde{\mathcal{H}}_5(G)$	$\tilde{\mathcal{H}}_6(G)$
70	power-bcspwr09	3.0977	4.5706	1723	174	159	191	202	48.6513	21.4249	11.6535	5.3691
71	power-bcspwr10	3.8988	6.5410	5300	721	700	657	856	142.2820	59.1038	22.2686	11.1898
72	copresence-InVS13	0.6581	6.2795	95	101236	13423	4047	453	1.0850	0.1567	0.3960	2.9278
73	hospital-ward-proximity	0.9636	7.3337	75	8215	12668	18992	23780	1.7594	0.3522	0.1105	0.0478
74	infect-hyper	0.9573	8.6923	113	16867	69350	278748	898126	1.7237	0.5806	0.2770	0.1572
75	primary-school-proximity	1.1019	15.6916	242	103760	760419	8321360	79399826	1.9171	0.5379	0.2968	0.1926
76	road City of Oldenburg	2.1546	2.4921	6105	41	124	72	101	20.1475	35.3207	11.1511	8.1694
77	road beijing	12.7863	18.6076	5036	153	780	187	154	44.8858	111.7337	12.2715	4.4477
78	road-chesapeake	0.9422	2.7193	39	194	839	228	116	1.7580	2.0670	0.1911	0.0424
79	road-euroroad	2.3307	3.0365	1039	32	38	52	43	12.1123	7.6863	5.2873	2.1171
80	road-minnesota	7.2982	9.5668	2640	53	54	47	52	20.3150	11.0617	4.8302	2.5772
81	tech-routers-rf	2.3901	6.7771	2113	10404	22816	22762	142077	252.3636	118.3659	23.7590	28.7436
82	email-dnc	2.5819	6.0927	1833	9431	16208	43358	153478	523.4261	253.3672	179.5366	162.1184
83	email-univ	1.7744	6.7378	1133	5343	12628	76309	598387	35.9839	12.0089	9.6973	9.8476
84	inf-USAir97	1.3100	5.5779	332	12181	4533	4110	5048	34.7915	1.4675	0.1475	0.0201
85	inf-euroroad	2.3747	3.0365	1039	32	38	52	43	12.1123	7.6863	5.2873	2.1171
86	inf-openflights	5.6518	21.8166	2905	72843	319407	1632910	11884654	349.7525	191.3919	114.9430	94.7289
87	inf-power	4.9972	6.9937	4941	651	324	311	331	205.4184	51.1473	23.0437	11.0593
88	london-overground	1.5239	1.7782	369	13	12	4	9	6.1614	3.3134	0.6087	0.7313
89	london-underground	1.5184	1.7520	271	10	11	3	8	4.9149	3.2085	0.4929	0.7195
90	web-EPA	3.7062	7.9616	4253	997	20160	20991	263470	81.6793	527.6272	164.7368	595.9513
91	web-indochina-2004	8.4246	28.5535	11358	210078	9187	503	482	2139.7439	14.9081	0.1220	0.0168
92	web-spam	3.2229	18.8184	4767	129017	1458084	18521029	320394705	200.7706	194.2912	198.8140	266.9143
93	web-webbase-2001	35.7642	60.9623	16062	21115	20420	8545	27865	3914.6051	1584.7703	260.3280	320.0004
94	soc-dolphins	1.3573	2.9995	62	95	59	142	239	4.2256	0.8408	0.6750	0.4042
95	soc-firm-hi-tech	0.9853	2.2311	33	77	35	69	42	2.7567	0.4717	0.4102	0.1323
96	soc-hamsterster	5.4328	29.9968	2000	52651	200462	2623585	36156328	75.7396	24.2996	25.3404	26.9436
97	soc-karate	1.3983	2.7736	34	45	36	20	2	2.7979	0.9341	0.2437	0.0132
98	soc-tribes	0.9268	2.1833	16	68	56	47	17	1.0754	0.7040	0.9233	1.0578
99	soc-wiki-Vote	2.4204	7.0649	889	2119	6873	25010	104736	45.1263	30.2818	21.5558	17.0979

Continued on next page

No.	*Name*	*RPMI*	*PMI*	*N*	$\lvert\mathcal{H}_3(G)\rvert$	$\lvert\mathcal{H}_4(G)\rvert$	$\lvert\mathcal{H}_5(G)\rvert$	$\lvert\mathcal{H}_6(G)\rvert$	$\tilde{\mathcal{H}}_3(G)$	$\tilde{\mathcal{H}}_4(G)$	$\tilde{\mathcal{H}}_5(G)$	$\tilde{\mathcal{H}}_6(G)$
100	fb-pages-food	3.0802	9.0002	620	2935	9003	12403	42583	57.3830	35.6805	9.4596	6.0761
101	fb-pages-politician	4.0911	18.9960	5908	174632	630811	2110870	11564939	372.3151	127.6622	38.1140	17.9313
102	fb-pages-public-figure	5.5812	25.4414	11565	184838	3384130	45669068	870671995	711.7478	1501.9709	2192.6066	4345.7187
103	fb-pages-tvshow	4.9838	18.2799	3892	87090	35915	31987	139241	751.6429	46.8912	5.9379	3.5371
104	socfb-Reed98	1.3020	16.6017	962	97137	1237142	26933744	562139763	9.7424	4.6062	3.6419	2.7654
105	socfb-nips-ego	1.5803	1.5279	2888	91	15	2	16	62.0595	6.6210	0.5362	2.5043
106	rt-retweet	1.3223	1.5292	96	12	14	3	4	4.9722	3.4143	0.4189	0.3185
107	rt-twitter-copen	1.8398	2.6331	761	149	183	349	697	45.2019	27.6401	24.7244	22.3428
108	rt-assad	3.4163	4.6820	2139	220	1629	4035	20053	74.6746	283.9715	339.2384	781.9029
109	rt-damascus	4.6052	6.0862	3052	165	1502	2542	17353	60.7439	291.4672	244.0459	792.1755
110	rt-obama	5.5761	5.7018	3212	14	199	60	656	8.6831	77.3844	13.7277	84.8579
111	rt-occupy	3.2230	4.1108	3225	115	725	1854	9776	47.3359	163.2345	214.2888	557.4450
112	rt-voteonedirection	12.5404	13.1401	2280	3	1899	12	26214	1.7826	698.0347	2.5616	3124.0963
113	C125-9	0.9957	10.9378	125	230619	191408	18995	204	1.0007	0.9798	1.0676	1.2001
114	MANN-a9	1.0522	3.7636	45	11244	2106	0	0	0.9938	1.2049	0.0000	0.0000
115	brock200-1	1.0031	28.7842	200	543700	3900964	7471673	3734928	0.9994	1.0046	0.9978	0.9804
116	gen200-p0-9-44	0.9929	16.8990	200	958030	1257669	177670	3788	1.0006	0.9878	0.9889	1.4416
117	johnson8-4-4	1.0894	10.9710	70	23940	73360	4032	3360	0.9650	1.4249	0.1549	1.0728
118	san200-0-9-1	0.9804	16.6245	200	960241	1215190	141944	822	1.0029	0.9544	0.7900	0.3128
119	bio-celegansneural	1.4051	7.1399	297	3241	15863	88393	625342	6.4256	3.2263	1.8241	1.3261
120	chesapeake	0.9266	2.7193	39	194	839	228	116	1.7580	2.0670	0.1911	0.0424
121	delaunay-n10	23.1244	63.3303	1024	2047	114	372	729	57.7590	0.7284	0.5081	0.2057
122	delaunay-n11	63.5916	174.7036	2048	4104	270	763	1414	114.9515	1.6968	1.0121	0.3813
123	insecta-ant-trophallaxis-colony1	1.0482	3.4683	41	445	1167	2807	4475	1.3719	0.8547	0.6837	0.5200
124	insecta-ant-trophallaxis-colony2	1.0662	3.4939	39	501	1114	2342	2868	1.5167	0.8431	0.6384	0.4157
125	mammalia-raccoon-proximity	0.7317	2.5290	24	1252	24	0	0	1.1267	0.0510	0.0000	0.0000
126	reptilia-tortoise-network-bsv	1.3165	3.2521	121	293	157	313	437	10.3557	1.4935	0.7943	0.3003

Continued on next page

No.	*Name*	*RPMI*	*PMI*	*N*	$\lvert\mathcal{H}_3(G)\rvert$	$\lvert\mathcal{H}_4(G)\rvert$	$\lvert\mathcal{H}_5(G)\rvert$	$\lvert\mathcal{H}_6(G)\rvert$	$\tilde{\mathcal{H}}_3(G)$	$\tilde{\mathcal{H}}_4(G)$	$\tilde{\mathcal{H}}_5(G)$	$\tilde{\mathcal{H}}_6(G)$
127	reptilia-tortoise-network-cs	1.0989	2.6022	31	96	63	44	32	2.6696	0.6518	0.2058	0.0843
128	reptilia-tortoise-network-fi	1.7979	3.6190	496	743	104	166	321	71.3693	3.4253	1.7753	1.0810
129	reptilia-tortoise-network-hw	1.4844	1.2667	6	0	1	0	0	0.0000	2.4113	0.0000	0.0000
130	reptilia-tortoise-network-lm	1.0986	2.2085	41	78	47	46	38	4.0344	0.9072	0.3634	0.1380
131	reptilia-tortoise-network-pv	1.0692	2.0606	22	51	0	0	0	3.4697	0.0000	0.0000	0.0000
132	DD199	62.5752	141.2739	841	1186	126	43	52	76.8959	2.4401	0.2347	0.0773
133	DD68	7.9454	20.5165	775	1472	333	261	551	56.0489	3.1824	0.5918	0.2869
134	DD687	4.7037	14.3214	725	2523	485	733	1726	41.0273	1.4998	0.4087	0.1685
135	citeseer	3.5091	6.4720	2110	1083	3058	3150	7511	154.6141	168.1378	62.6671	52.0142
136	cora	2.4179	5.0657	2485	1558	1523	1840	4752	137.6707	44.1636	16.4488	12.5980
137	gene	1.7007	3.1640	814	809	180	92	135	110.5148	9.3966	1.7302	0.8830
138	internet-industry-partnerships	1.3454	3.5067	219	328	1434	3950	11671	10.3337	11.1475	7.3295	5.1209
139	webkb-wisc	2.1146	3.8737	251	118	359	95	69	15.3580	18.0282	1.7579	0.4601
140	tech-WHOIS	3.5623	17.3702	7476	782494	2934453	31835788	397659584	1328.0945	437.8254	392.3110	389.3882

17

Table S3. Correlations between network metrics and PMI/RPMI.

	PMI			RPMI		
	ρ_p	ρ_s	QCR	ρ_p	ρ_s	QCR
$\tilde{\mathcal{H}}_3(G)$	0.2303	0.3314	0.6286	0.2638	0.7153	0.9000
$\tilde{\mathcal{H}}_4(G)$	0.1486	0.3339	0.6000	0.2397	0.8417	0.8857
$\tilde{\mathcal{H}}_5(G)$	0.0609	0.3727	0.6286	0.0486	0.6735	0.8429
$\tilde{\mathcal{H}}_6(G)$	0.0241	0.3714	0.6429	0.0703	0.6971	0.8000
n_c	0.1612	0.2403	0.6286	0.2304	0.8497	0.9857
$\langle k \rangle$	0.1144	0.4983	0.6714	-0.1246	-0.4846	0.6714
L	0.1570	-0.0044	0.5000	0.3007	0.7912	0.8429
E_{glob}	-0.1595	-0.0518	0.5286	-0.3164	-0.8208	0.8714
D	0.1658	0.0462	0.5429	0.3106	0.8109	0.8571
r	0.1668	0.2003	0.5899	0.1065	0.2061	0.5571
C	0.0893	0.2172	0.5571	-0.0855	-0.5981	0.7429
k_s	0.1652	0.6377	0.7429	-0.0765	-0.1952	0.5657

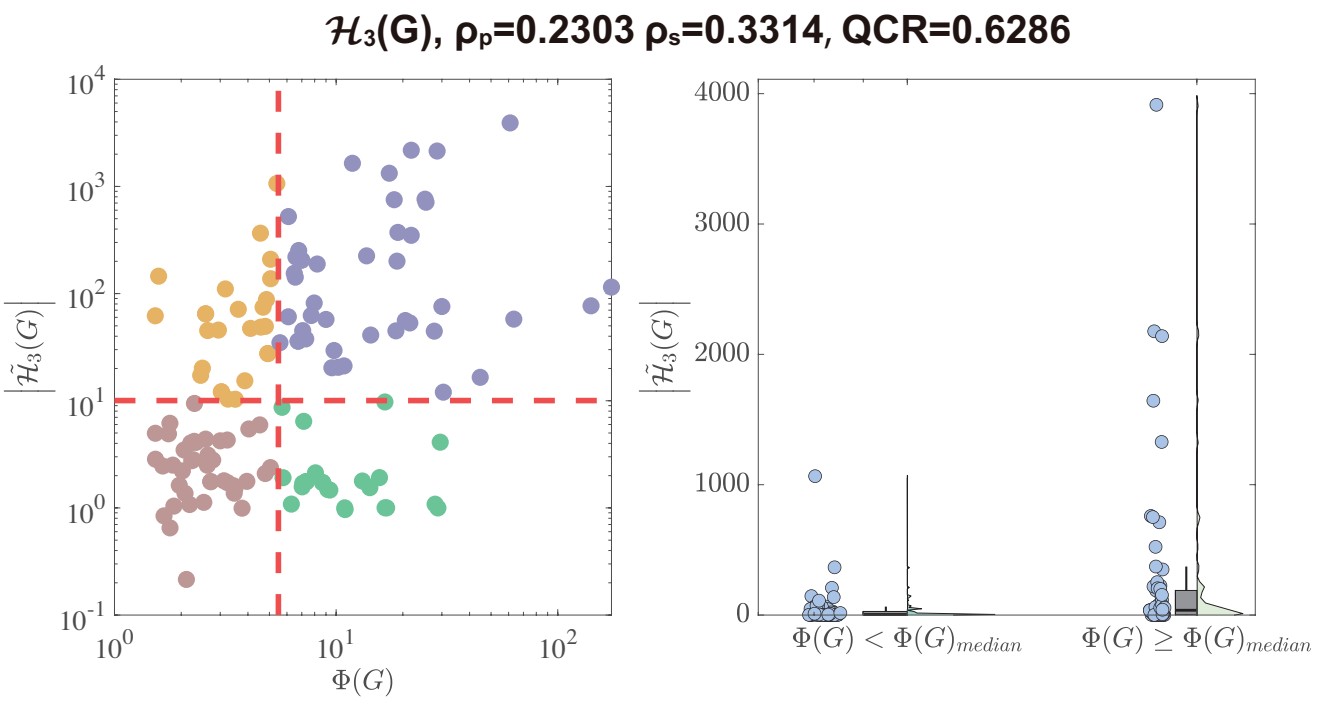

Fig. S1. Correlation between path multiplicity and chordless 3-cycles in 140 real-world networks. The metadata and results for all 140 networks are given in Supplementary Materials. **a,** The left part of each panel presents a scatter plot along with the Pearson correlation ρ between $\Phi(G)$ and $|\tilde{\mathcal{H}}_3(G)|$. Each scatter plot is divided into four quadrants by the median values of $\Phi(G)$ and $|\tilde{\mathcal{H}}_3(G)|$ and the Quadrant Count Ratio (QCR) is also shown. The right-hand violin plots show the distribution, mean and median values of the corresponding $|\tilde{\mathcal{H}}_3(G)|$, which are divided into two parts based on the median value of PMI. If there are more overlap between two violin subplots, it suggests a weaker correlation between a specific chordless cycle and PMI.

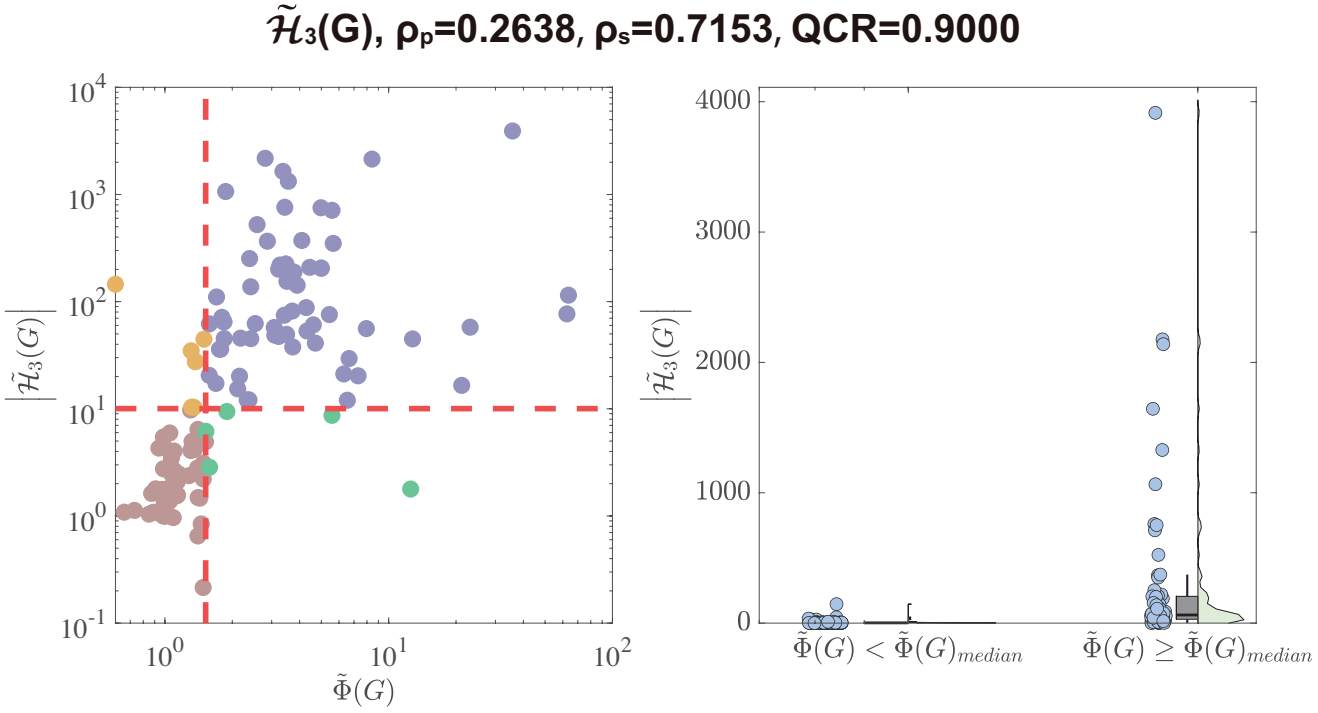

Fig. S2. Correlation between relative path multiplicity and chordless 3-cycles in 140 real-world networks. The metadata and results for all 140 networks are given in Supplementary Materials. **a,** The left part of each panel presents a scatter plot along with the Pearson correlation ρ between $\tilde{\Phi}(G)$ and $|\tilde{\mathcal{H}}_3(G)|$. Each scatter plot is divided into four quadrants by the median values of $\tilde{\Phi}(G)$ and $|\tilde{\mathcal{H}}_3(G)|$ and the Quadrant Count Ratio (QCR) is also shown. The right-hand violin plots show the distribution, mean and median values of the corresponding $|\tilde{\mathcal{H}}_3(G)|$, which are divided into two parts based on the median value of RPMI. If there are more overlap between two violin subplots, it suggests a weaker correlation between a specific chordless cycle and RPMI.

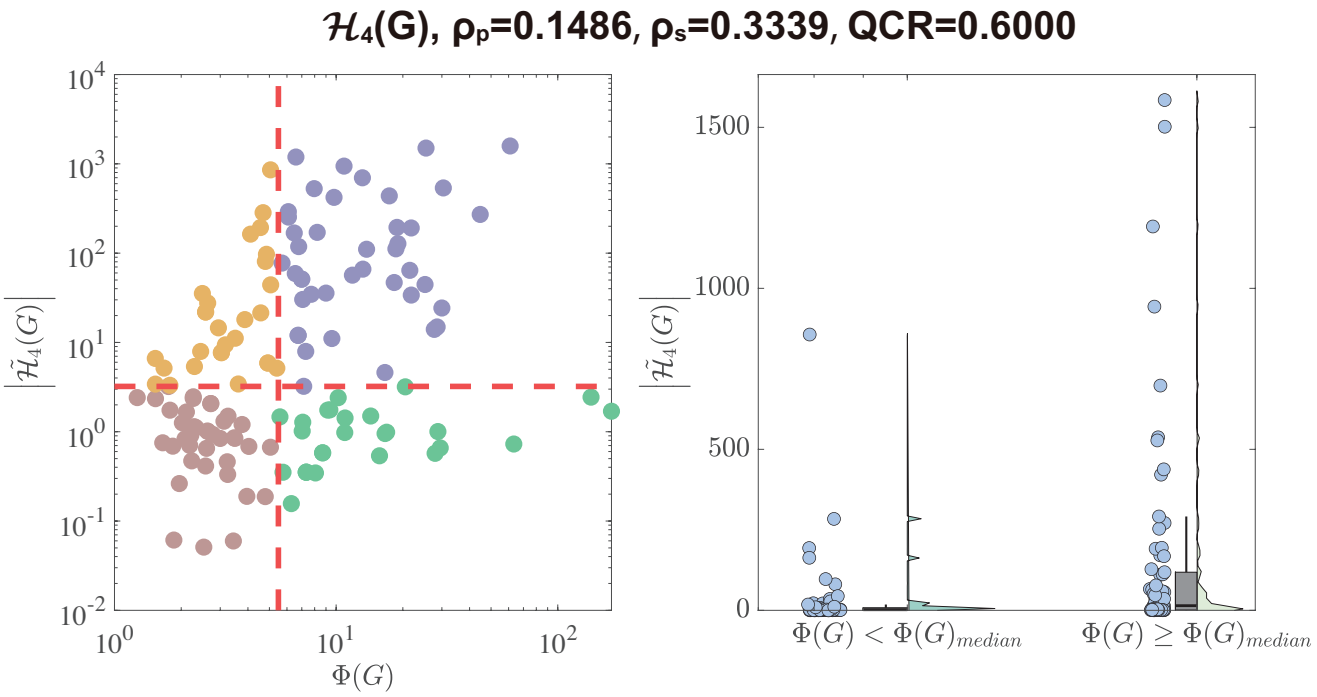

Fig. S3. Correlation between path multiplicity and chordless 4-cycles in 140 real-world networks. The metadata and results for all 140 networks are given in Supplementary Materials. **a,** The left part of each panel presents a scatter plot along with the Pearson correlation ρ between $\Phi(G)$ and $|\tilde{\mathcal{H}}_4(G)|$. Each scatter plot is divided into four quadrants by the median values of $\Phi(G)$ and $|\tilde{\mathcal{H}}_4(G)|$ and the Quadrant Count Ratio (QCR) is also shown. The right-hand violin plots show the distribution, mean and median values of the corresponding $|\tilde{\mathcal{H}}_4(G)|$, which are divided into two parts based on the median value of PMI. If there are more overlap between two violin subplots, it suggests a weaker correlation between a specific chordless cycle and PMI.

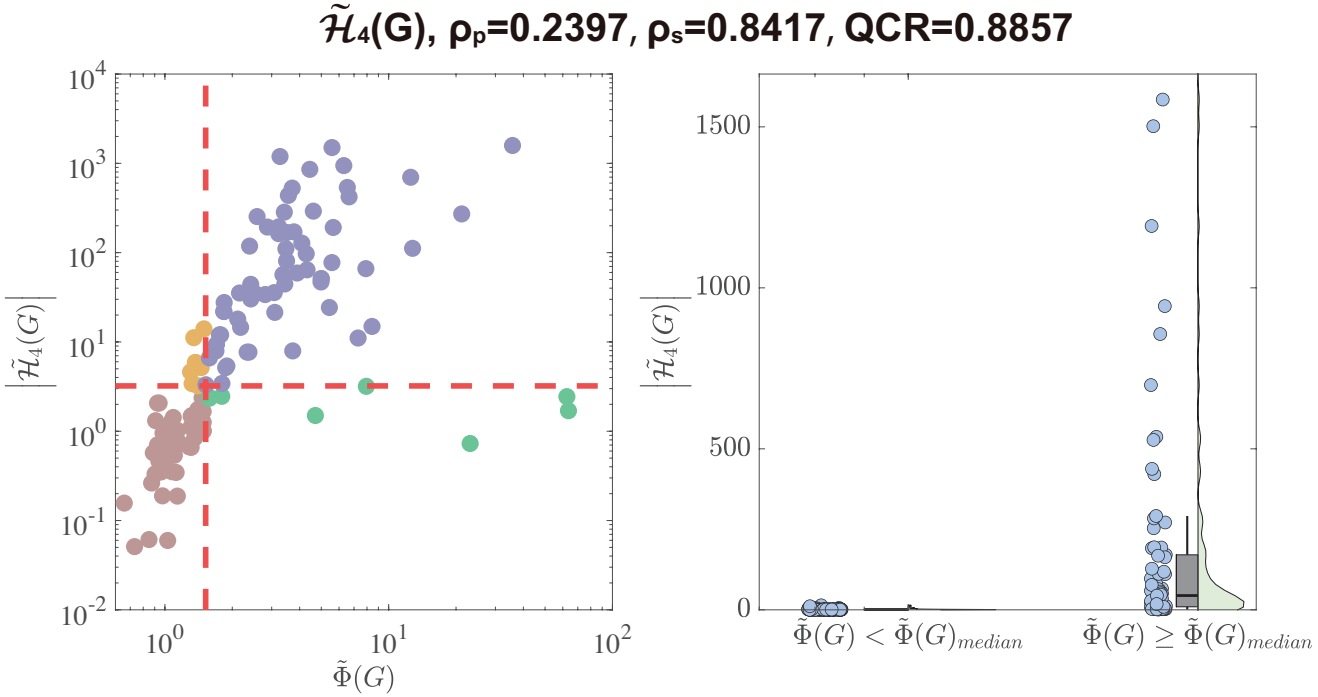

Fig. S4. Correlation between relative path multiplicity and chordless 4-cycles in 140 real-world networks. The metadata and results for all 140 networks are given in Supplementary Materials. **a,** The left part of each panel presents a scatter plot along with the Pearson correlation ρ between $\tilde{\Phi}(G)$ and $|\tilde{\mathcal{H}}_4(G)|$. Each scatter plot is divided into four quadrants by the median values of $\tilde{\Phi}(G)$ and $|\tilde{\mathcal{H}}_4(G)|$ and the Quadrant Count Ratio (QCR) is also shown. The right-hand violin plots show the distribution, mean and median values of the corresponding $|\tilde{\mathcal{H}}_4(G)|$, which are divided into two parts based on the median value of RPMI. If there are more overlap between two violin subplots, it suggests a weaker correlation between a specific chordless cycle and RPMI.

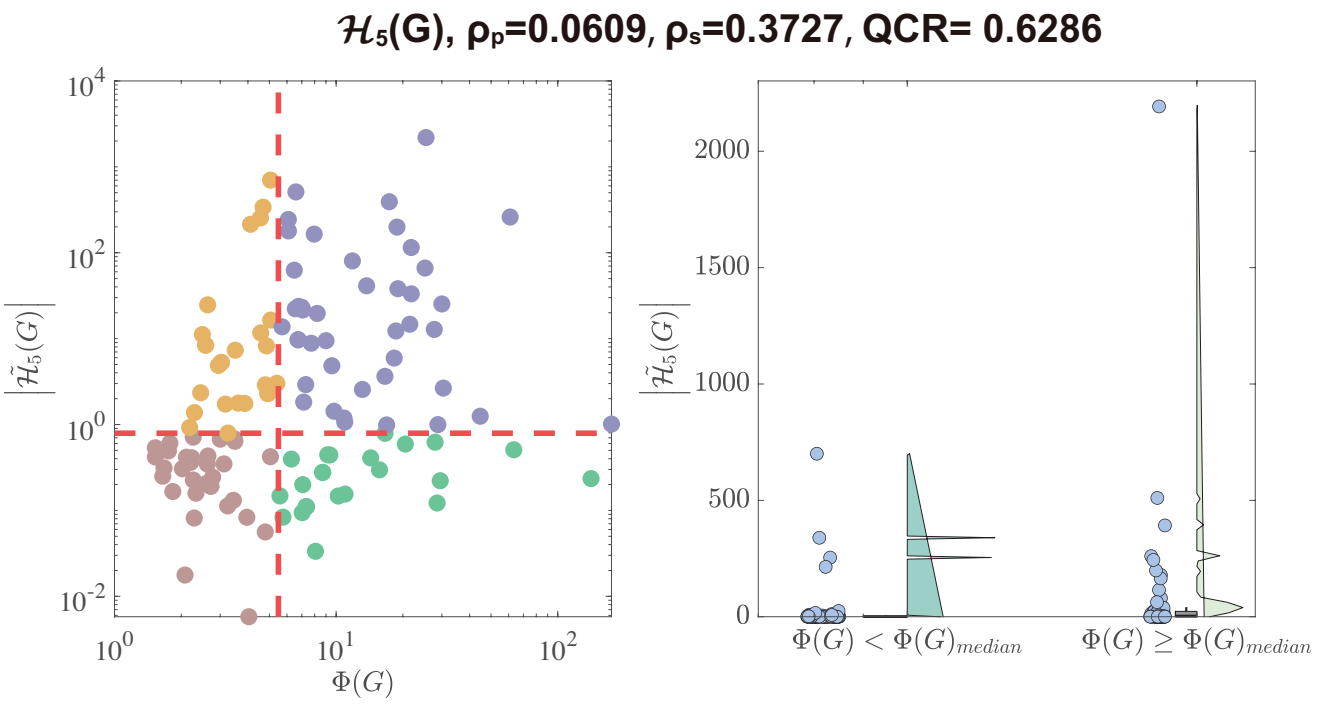

Fig. S5. Correlation between path multiplicity and chordless 5-cycles in 140 real-world networks. The metadata and results for all 140 networks are given in Supplementary Materials. **a,** The left part of each panel presents a scatter plot along with the Pearson correlation ρ between $\Phi(G)$ and $|\tilde{\mathcal{H}}_5(G)|$. Each scatter plot is divided into four quadrants by the median values of $\Phi(G)$ and $|\tilde{\mathcal{H}}_5(G)|$ and the Quadrant Count Ratio (QCR) is also shown. The right-hand violin plots show the distribution, mean and median values of the corresponding $|\tilde{\mathcal{H}}_5(G)|$, which are divided into two parts based on the median value of PMI. If there are more overlap between two violin subplots, it suggests a weaker correlation between a specific chordless cycle and PMI.

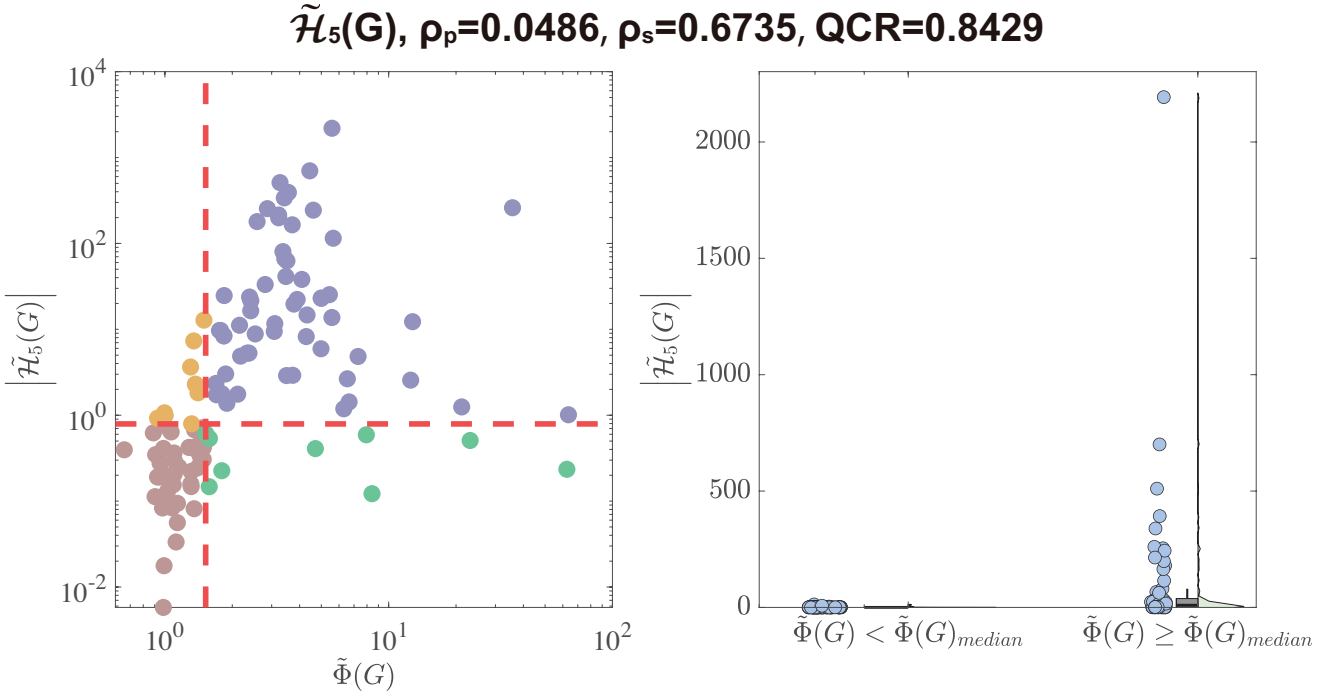

Fig. S6. Correlation between relative path multiplicity and chordless 5-cycles in 140 real-world networks. The metadata and results for all 140 networks are given in Supplementary Materials. **a,** The left part of each panel presents a scatter plot along with the Pearson correlation ρ between $\tilde{\Phi}(G)$ and $|\tilde{\mathcal{H}}_5(G)|$. Each scatter plot is divided into four quadrants by the median values of $\tilde{\Phi}(G)$ and $|\tilde{\mathcal{H}}_5(G)|$ and the Quadrant Count Ratio (QCR) is also shown. The right-hand violin plots show the distribution, mean and median values of the corresponding $|\tilde{\mathcal{H}}_5(G)|$, which are divided into two parts based on the median value of RPMI. If there are more overlap between two violin subplots, it suggests a weaker correlation between a specific chordless cycle and RPMI.

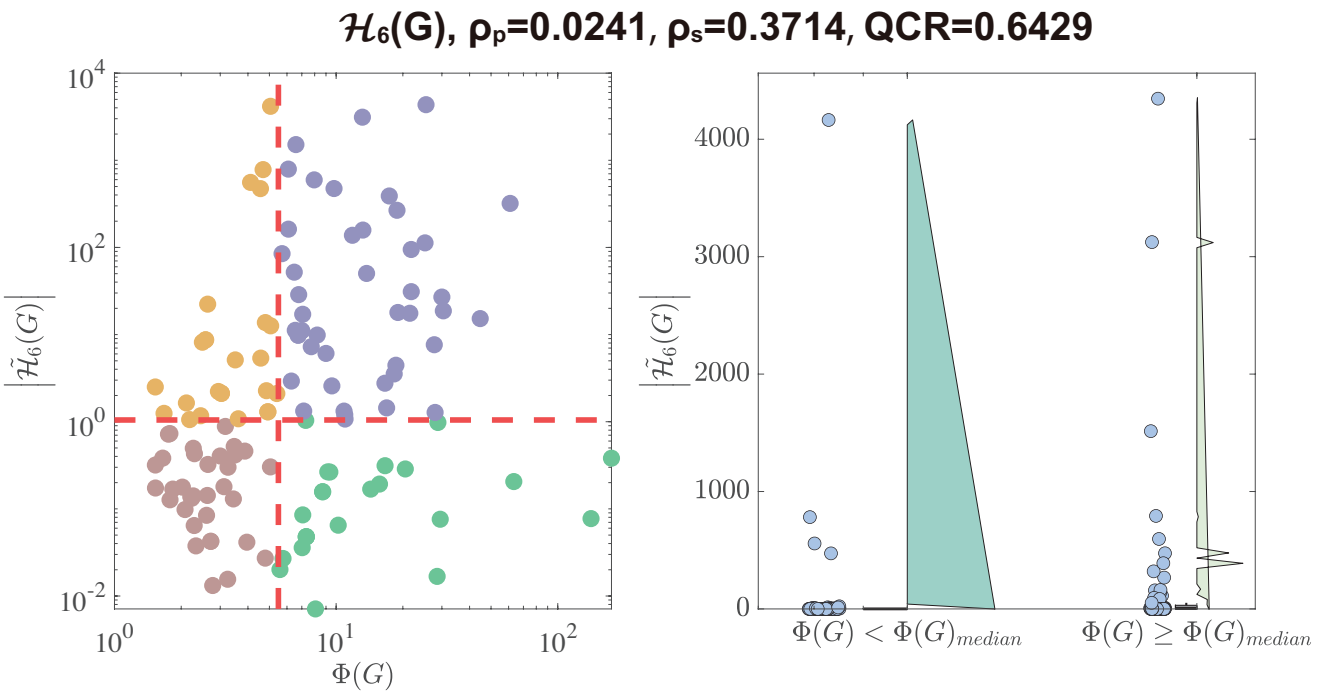

Fig. S7. Correlation between path multiplicity and chordless 6-cycles in 140 real-world networks. The metadata and results for all 140 networks are given in Supplementary Materials. **a,** The left part of each panel presents a scatter plot along with the Pearson correlation ρ between $\Phi(G)$ and $|\tilde{\mathcal{H}}_6(G)|$. Each scatter plot is divided into four quadrants by the median values of $\Phi(G)$ and $|\tilde{\mathcal{H}}_6(G)|$ and the Quadrant Count Ratio (QCR) is also shown. The right-hand violin plots show the distribution, mean and median values of the corresponding $|\tilde{\mathcal{H}}_6(G)|$, which are divided into two parts based on the median value of PMI. If there are more overlap between two violin subplots, it suggests a weaker correlation between a specific chordless cycle and PMI.

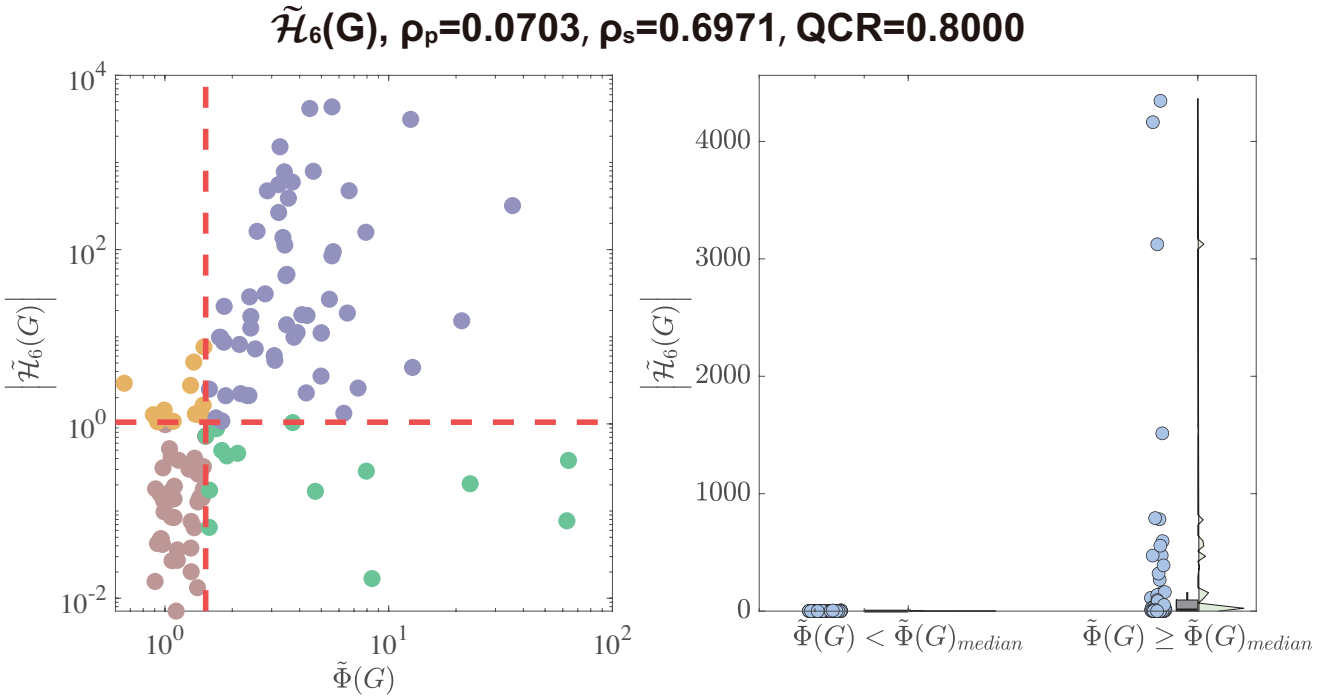

Fig. S8. Correlation between relative path multiplicity and chordless 6-cycles in 140 real-world networks. The metadata and results for all 140 networks are given in Supplementary Materials. **a,** The left part of each panel presents a scatter plot along with the Pearson correlation ρ between $\tilde{\Phi}(G)$ and $|\tilde{\mathcal{H}}_6(G)|$. Each scatter plot is divided into four quadrants by the median values of $\tilde{\Phi}(G)$ and $|\tilde{\mathcal{H}}_6(G)|$ and the Quadrant Count Ratio (QCR) is also shown. The right-hand violin plots show the distribution, mean and median values of the corresponding $|\tilde{\mathcal{H}}_6(G)|$, which are divided into two parts based on the median value of RPMI. If there are more overlap between two violin subplots, it suggests a weaker correlation between a specific chordless cycle and RPMI.

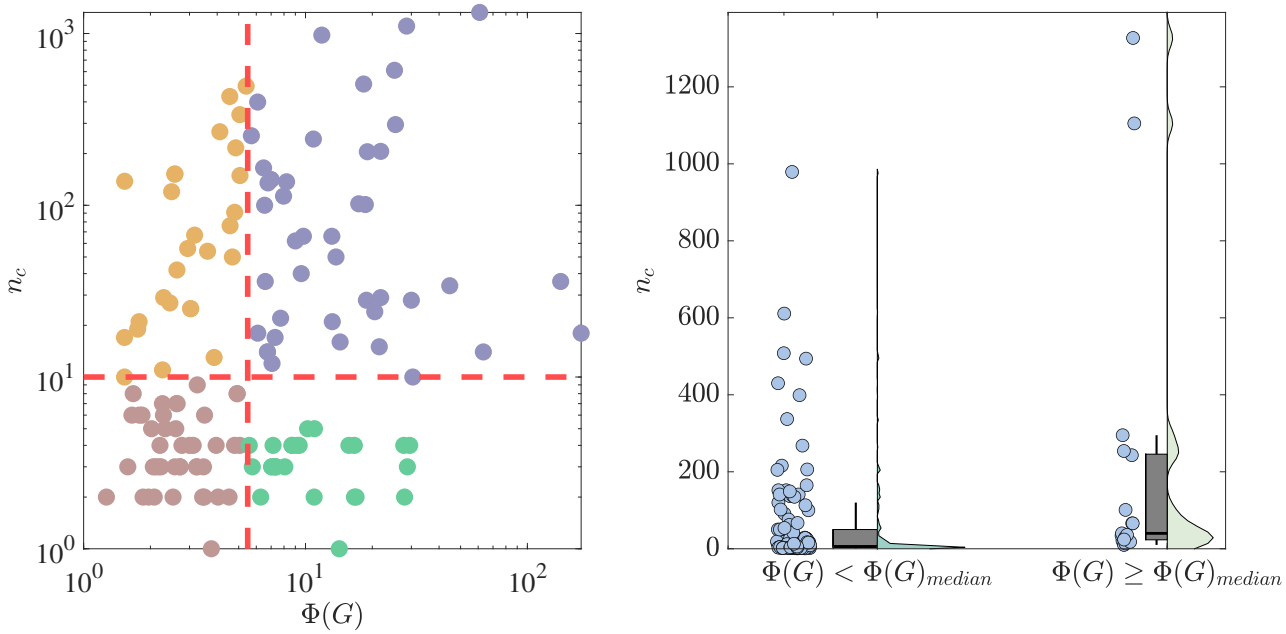

Fig. S9. Correlation between path multiplicity and community number in 140 real-world networks. The metadata and results for all 140 networks are given in Supplementary Materials. **a,** The left part of each panel presents a scatter plot along with the Pearson correlation ρ between $\Phi(G)$ and n_c. Each scatter plot is divided into four quadrants by the median values of $\Phi(G)$ and n_c and the Quadrant Count Ratio (QCR) is also shown. The right-hand violin plots show the distribution, mean and median values of the corresponding n_c, which are divided into two parts based on the median value of PMI. If there are more overlap between two violin subplots, it suggests a weaker correlation between the corresponding network metric and PMI.

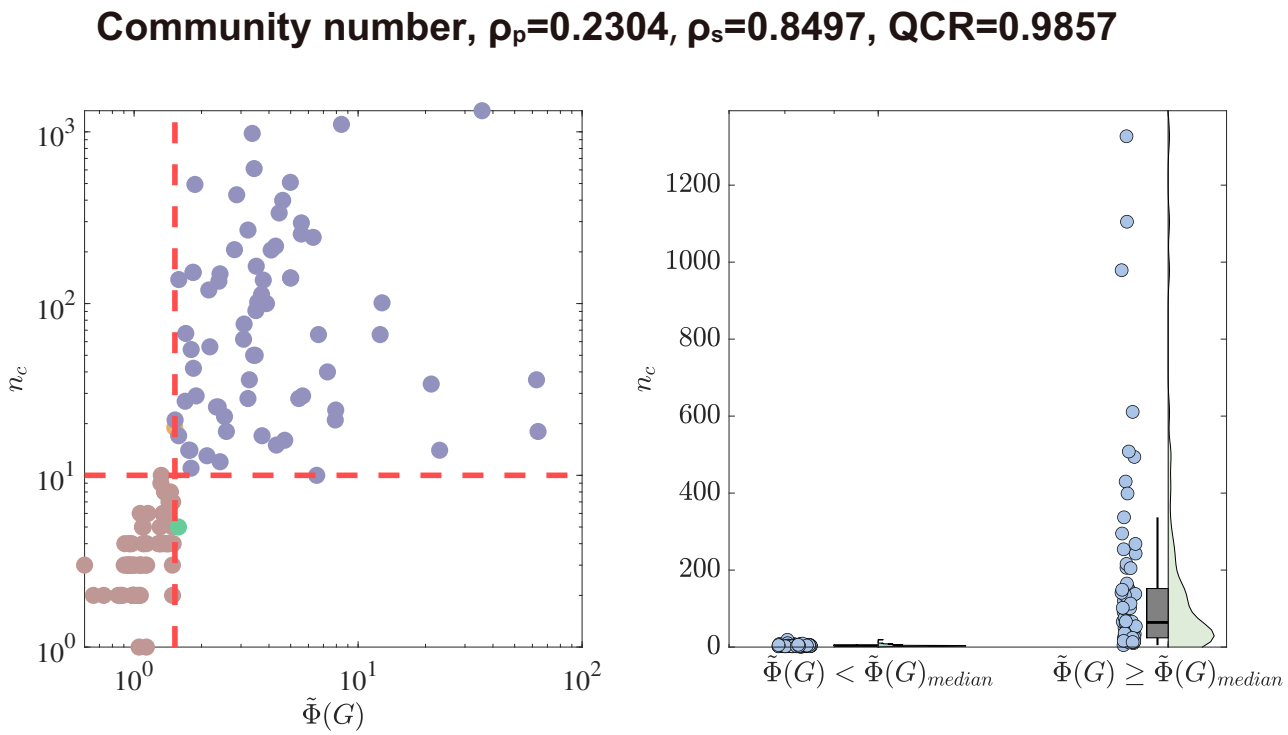

Fig. S10. Correlation between relative path multiplicity and community number in 140 real-world networks. The metadata and results for all 140 networks are given in Supplementary Materials. **a,** The left part of each panel presents a scatter plot along with the Pearson correlation ρ between $\tilde{\Phi}(G)$ and n_c. Each scatter plot is divided into four quadrants by the median values of $\tilde{\Phi}(G)$ and n_c and the Quadrant Count Ratio (QCR) is also shown. The right-hand violin plots show the distribution, mean and median values of the corresponding n_c, which are divided into two parts based on the median value of RPMI. If there are more overlap between two violin subplots, it suggests a weaker correlation between the corresponding network metric and RPMI.

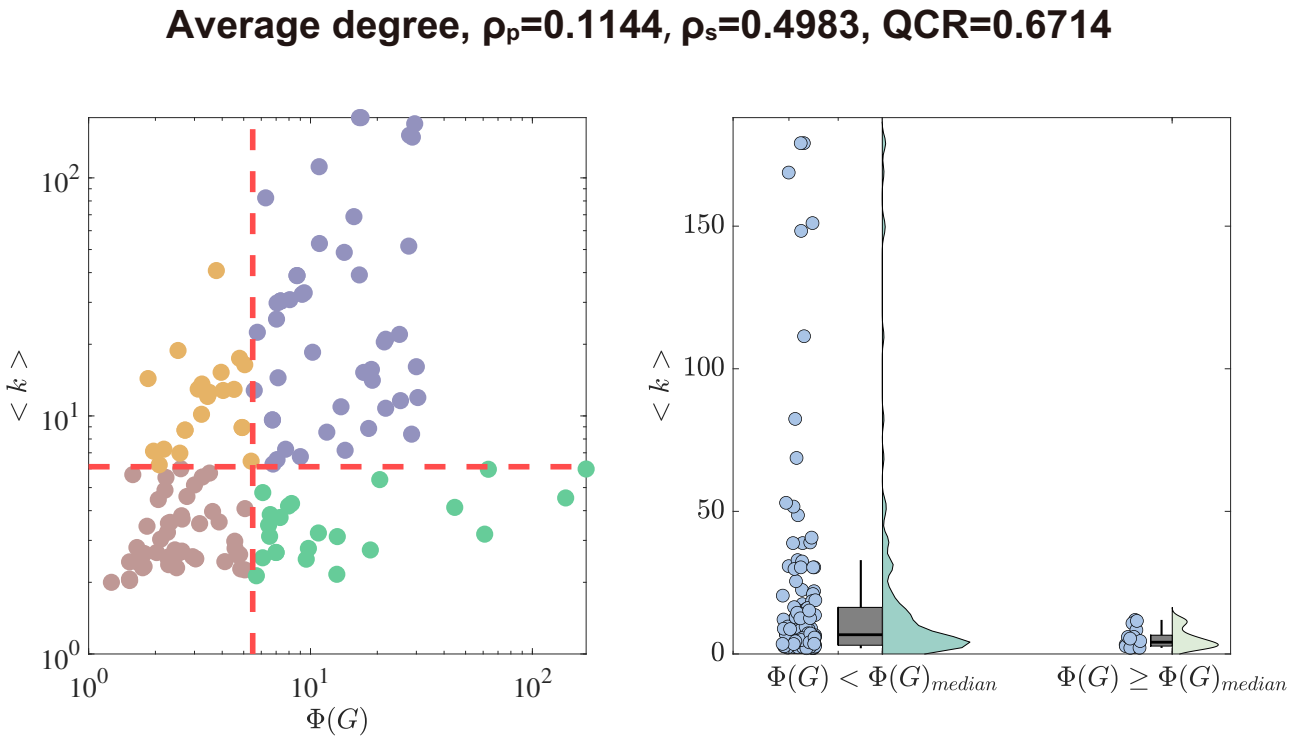

Fig. S11. Correlation between path multiplicity and average degree in 140 real-world networks. The metadata and results for all 140 networks are given in Supplementary Materials. **a,** The left part of each panel presents a scatter plot along with the Pearson correlation ρ between $\Phi(G)$ and $< k >$. Each scatter plot is divided into four quadrants by the median values of $\Phi(G)$ and $< k >$ and the Quadrant Count Ratio (QCR) is also shown. The right-hand violin plots show the distribution, mean and median values of the corresponding $< k >$, which are divided into two parts based on the median value of PMI. If there are more overlap between two violin subplots, it suggests a weaker correlation between the corresponding network metric and PMI.

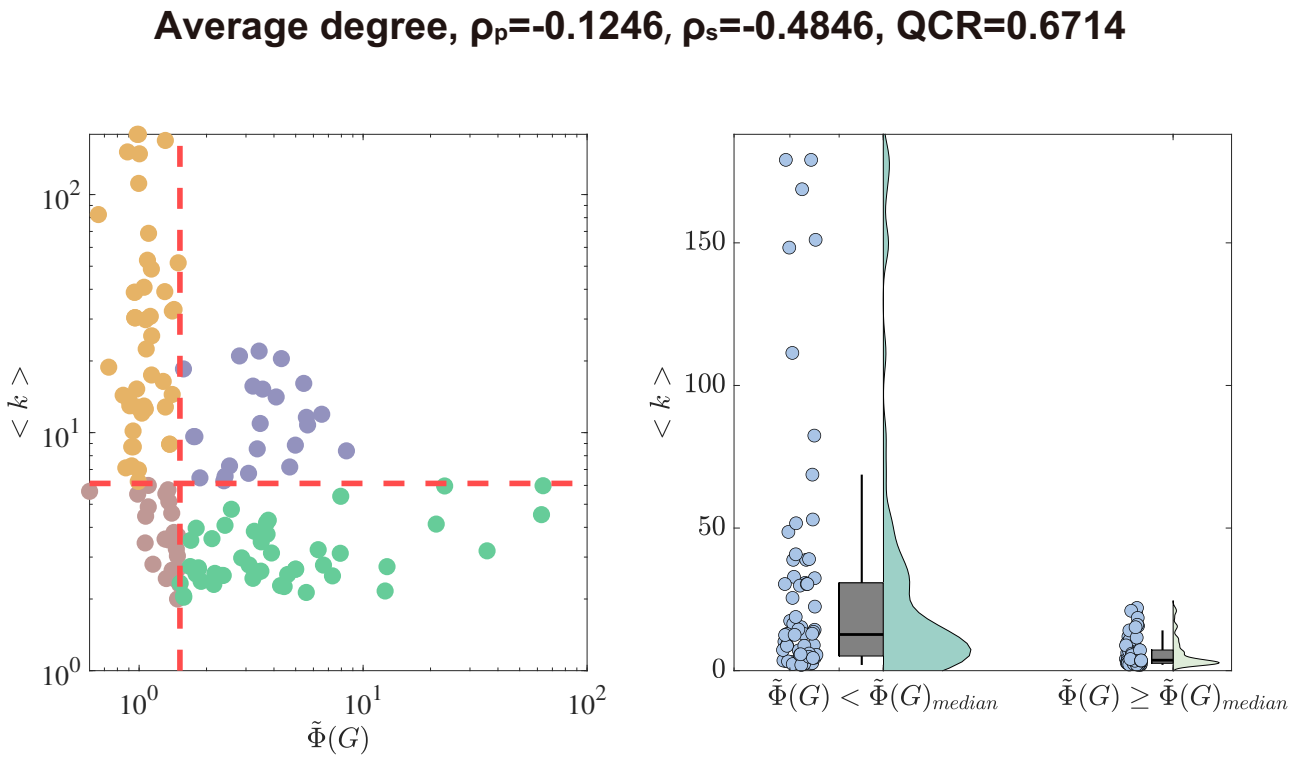

Fig. S12. Correlation between relative path multiplicity and average degree in 140 real-world networks. The metadata and results for all 140 networks are given in Supplementary Materials. **a,** The left part of each panel presents a scatter plot along with the Pearson correlation ρ between $\tilde{\Phi}(G)$ and $< k >$. Each scatter plot is divided into four quadrants by the median values of $\tilde{\Phi}(G)$ and $< k >$ and the Quadrant Count Ratio (QCR) is also shown. The right-hand violin plots show the distribution, mean and median values of the corresponding $< k >$, which are divided into two parts based on the median value of RPMI. If there are more overlap between two violin subplots, it suggests a weaker correlation between the corresponding network metric and RPMI.

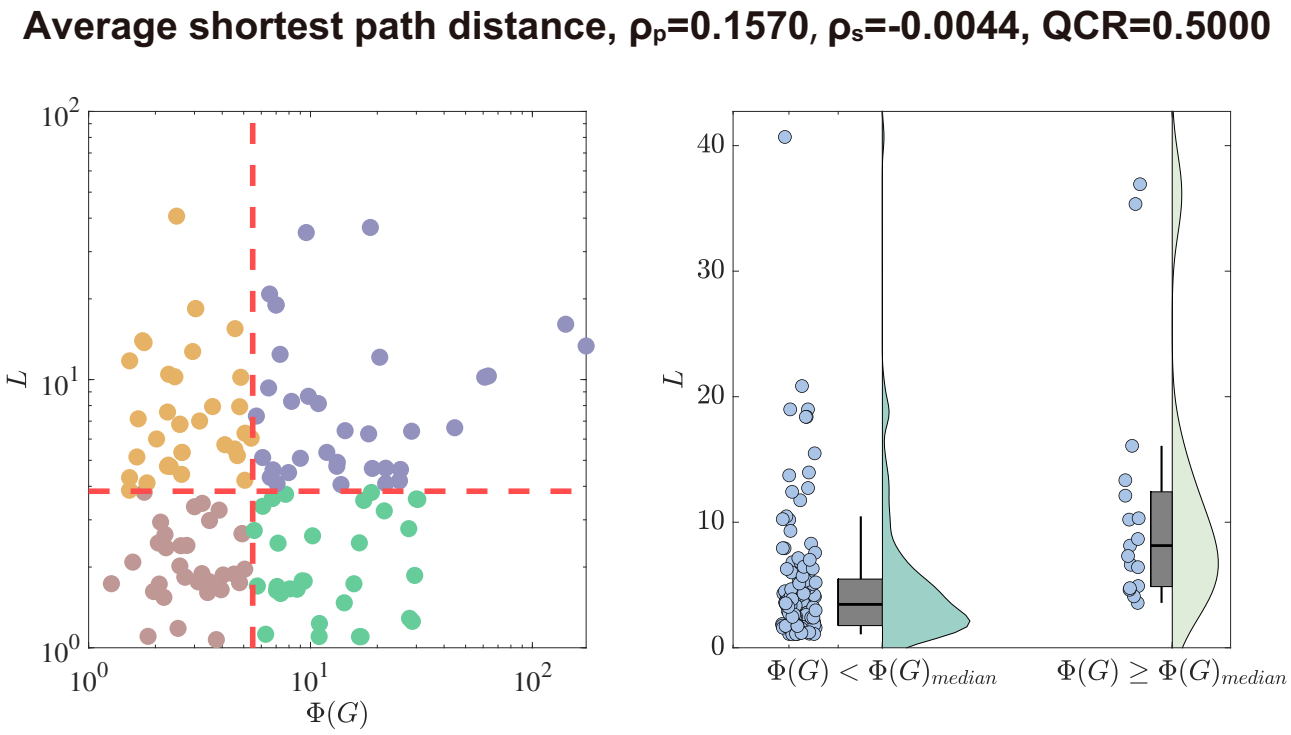

Fig. S13. Correlation between path multiplicity and average shortest path distance in 140 real-world networks. The metadata and results for all 140 networks are given in Supplementary Materials. **a,** The left part of each panel presents a scatter plot along with the Pearson correlation ρ between $\Phi(G)$ and L. Each scatter plot is divided into four quadrants by the median values of $\Phi(G)$ and L and the Quadrant Count Ratio (QCR) is also shown. The right-hand violin plots show the distribution, mean and median values of the corresponding L, which are divided into two parts based on the median value of PMI. If there are more overlap between two violin subplots, it suggests a weaker correlation between the corresponding network metric and PMI.

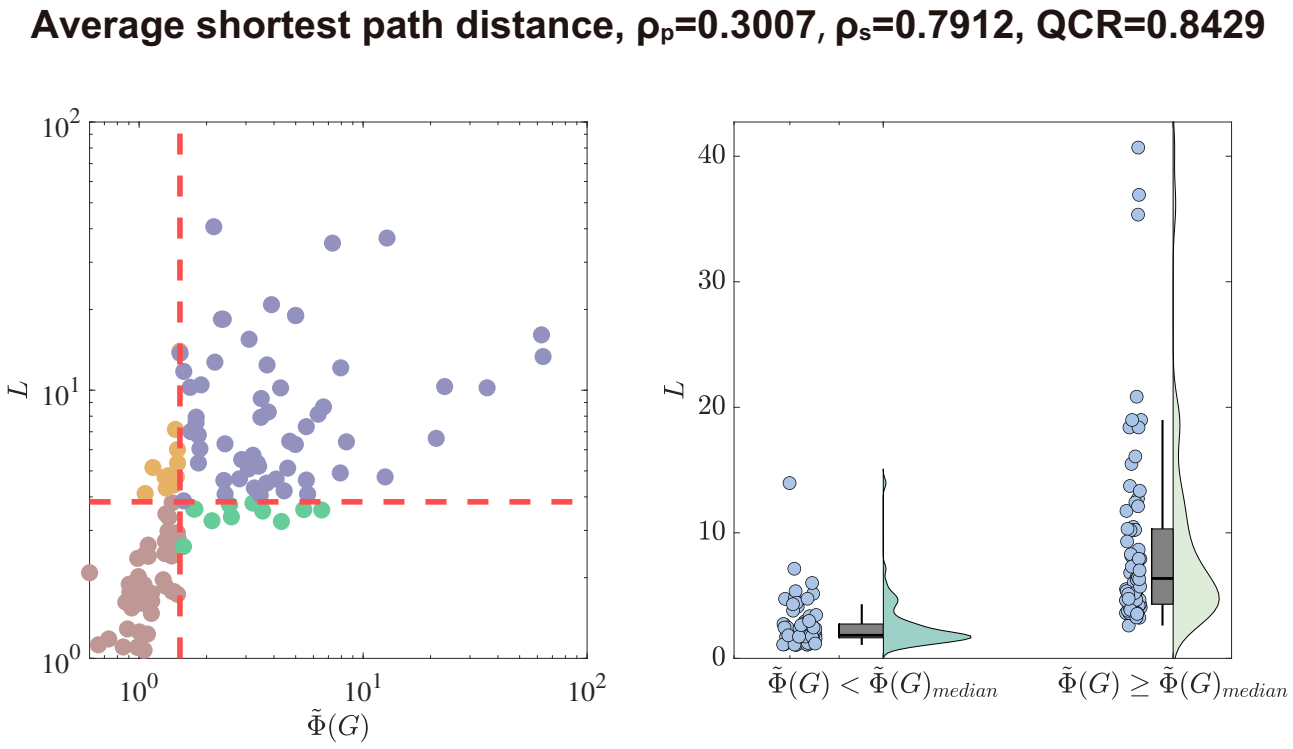

Fig. S14. Correlation between relative path multiplicity and average shortest path distance in 140 real-world networks. The metadata and results for all 140 networks are given in Supplementary Materials. **a,** The left part of each panel presents a scatter plot along with the Pearson correlation ρ between $\tilde{\Phi}(G)$ and L. Each scatter plot is divided into four quadrants by the median values of $\tilde{\Phi}(G)$ and L and the Quadrant Count Ratio (QCR) is also shown. The right-hand violin plots show the distribution, mean and median values of the corresponding L, which are divided into two parts based on the median value of RPMI. If there are more overlap between two violin subplots, it suggests a weaker correlation between the corresponding network metric and RPMI.

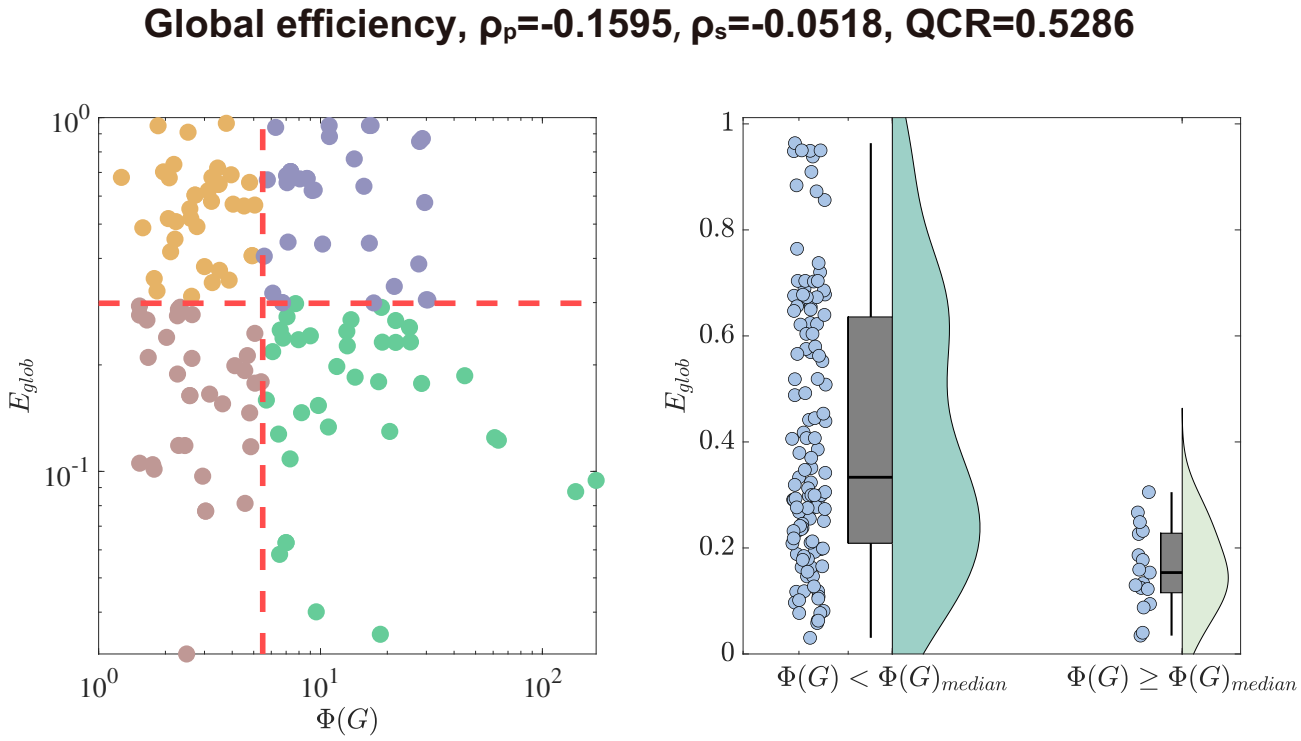

Fig. S15. Correlation between path multiplicity and global efficiency in 140 real-world networks. The metadata and results for all 140 networks are given in Supplementary Materials. **a,** The left part of each panel presents a scatter plot along with the Pearson correlation ρ between $\Phi(G)$ and E_{glob}. Each scatter plot is divided into four quadrants by the median values of $\Phi(G)$ and E_{glob} and the Quadrant Count Ratio (QCR) is also shown. The right-hand violin plots show the distribution, mean and median values of the corresponding E_{glob}, which are divided into two parts based on the median value of PMI. If there are more overlap between two violin subplots, it suggests a weaker correlation between the corresponding network metric and PMI.

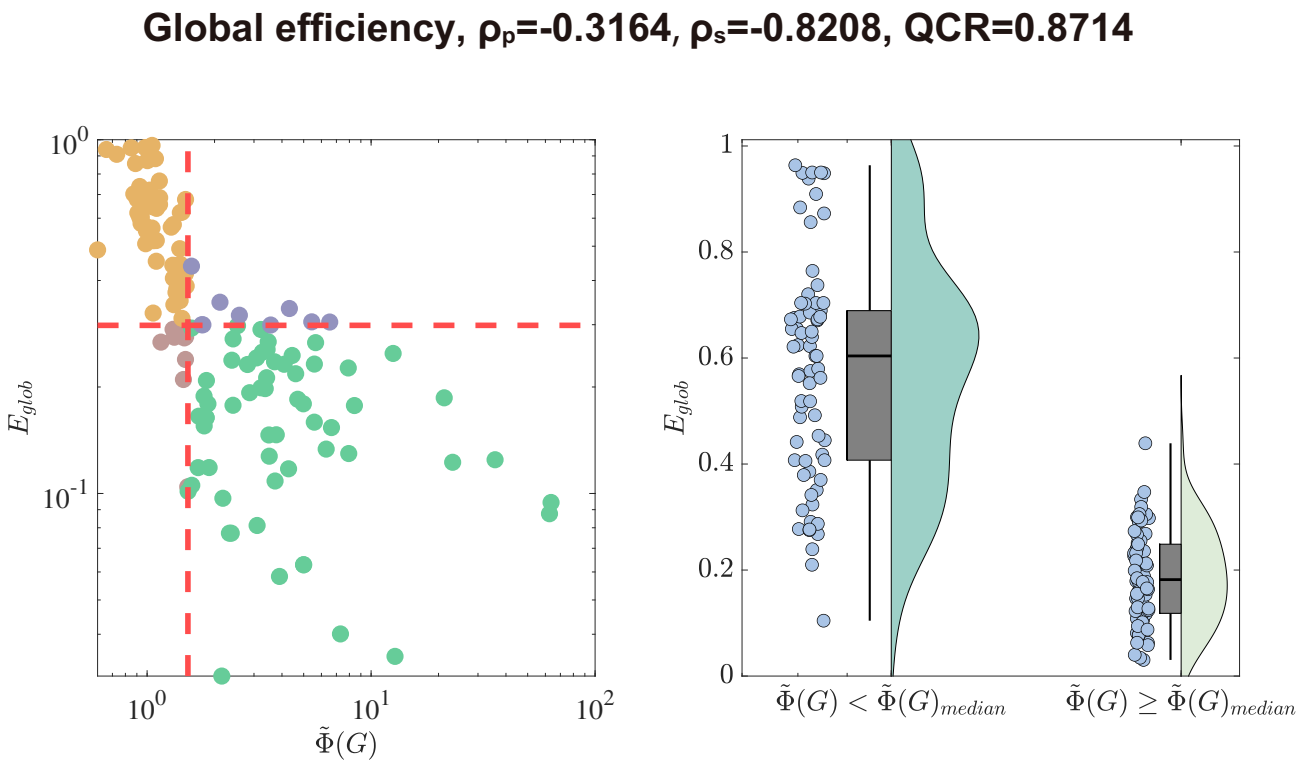

Fig. S16. Correlation between relative path multiplicity and global efficiency in 140 real-world networks. The metadata and results for all 140 networks are given in Supplementary Materials. **a,** The left part of each panel presents a scatter plot along with the Pearson correlation ρ between $\tilde{\Phi}(G)$ and E_{glob}. Each scatter plot is divided into four quadrants by the median values of $\tilde{\Phi}(G)$ and E_{glob} and the Quadrant Count Ratio (QCR) is also shown. The right-hand violin plots show the distribution, mean and median values of the corresponding E_{glob}, which are divided into two parts based on the median value of RPMI. If there are more overlap between two violin subplots, it suggests a weaker correlation between the corresponding network metric and RPMI.

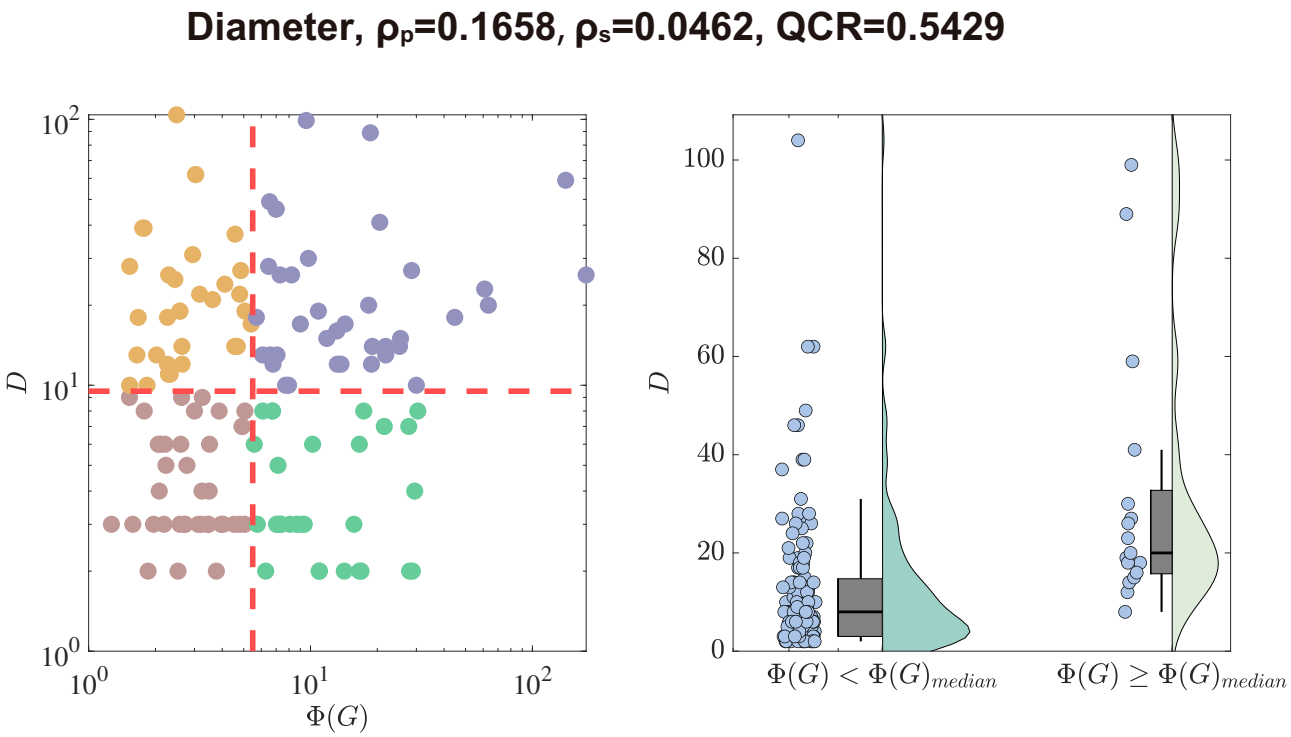

Fig. S17. Correlation between path multiplicity and diameter in 140 real-world networks. The metadata and results for all 140 networks are given in Supplementary Materials. **a,** The left part of each panel presents a scatter plot along with the Pearson correlation ρ between $\Phi(G)$ and D. Each scatter plot is divided into four quadrants by the median values of $\Phi(G)$ and D and the Quadrant Count Ratio (QCR) is also shown. The right-hand violin plots show the distribution, mean and median values of the corresponding D, which are divided into two parts based on the median value of PMI. If there are more overlap between two violin subplots, it suggests a weaker correlation between the corresponding network metric and PMI.

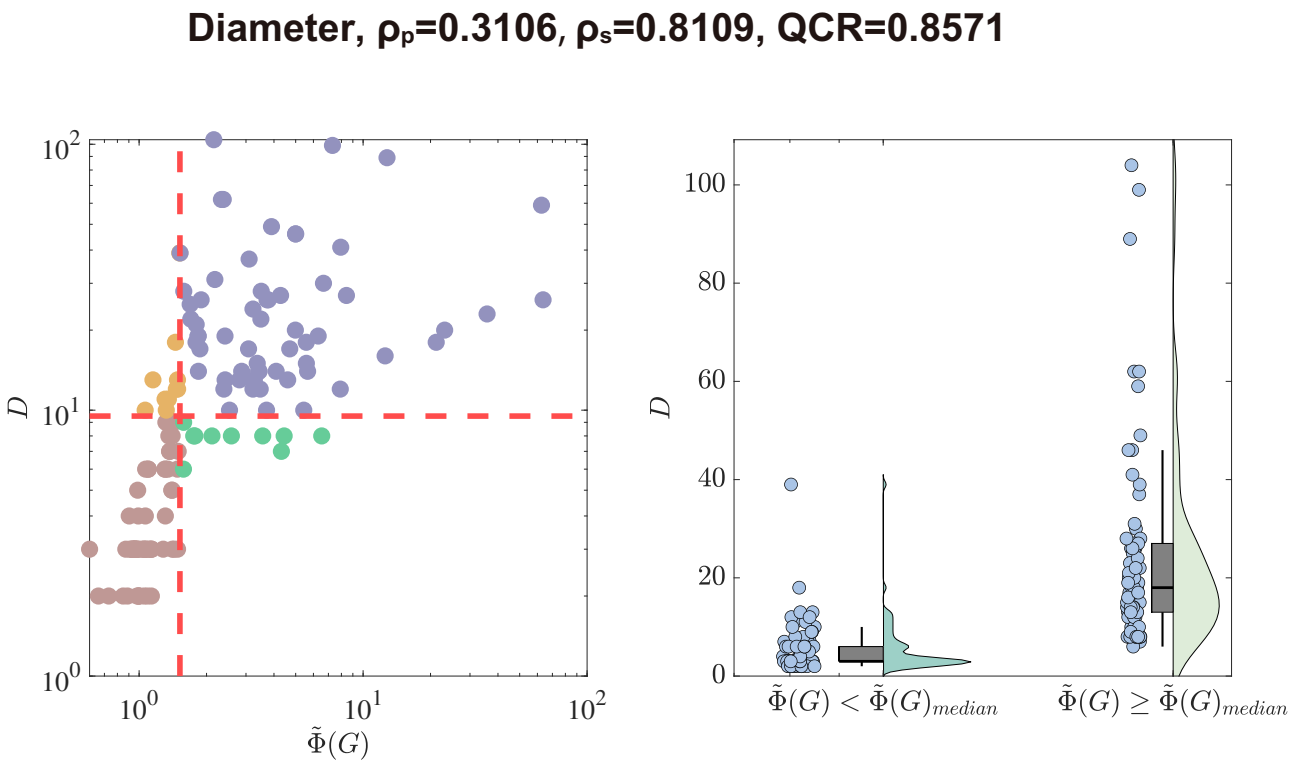

Fig. S18. Correlation between relative path multiplicity and diameter in 140 real-world networks. The metadata and results for all 140 networks are given in Supplementary Materials. **a,** The left part of each panel presents a scatter plot along with the Pearson correlation ρ between $\tilde{\Phi}(G)$ and D. Each scatter plot is divided into four quadrants by the median values of $\tilde{\Phi}(G)$ and D and the Quadrant Count Ratio (QCR) is also shown. The right-hand violin plots show the distribution, mean and median values of the corresponding D, which are divided into two parts based on the median value of RPMI. If there are more overlap between two violin subplots, it suggests a weaker correlation between the corresponding network metric and RPMI.

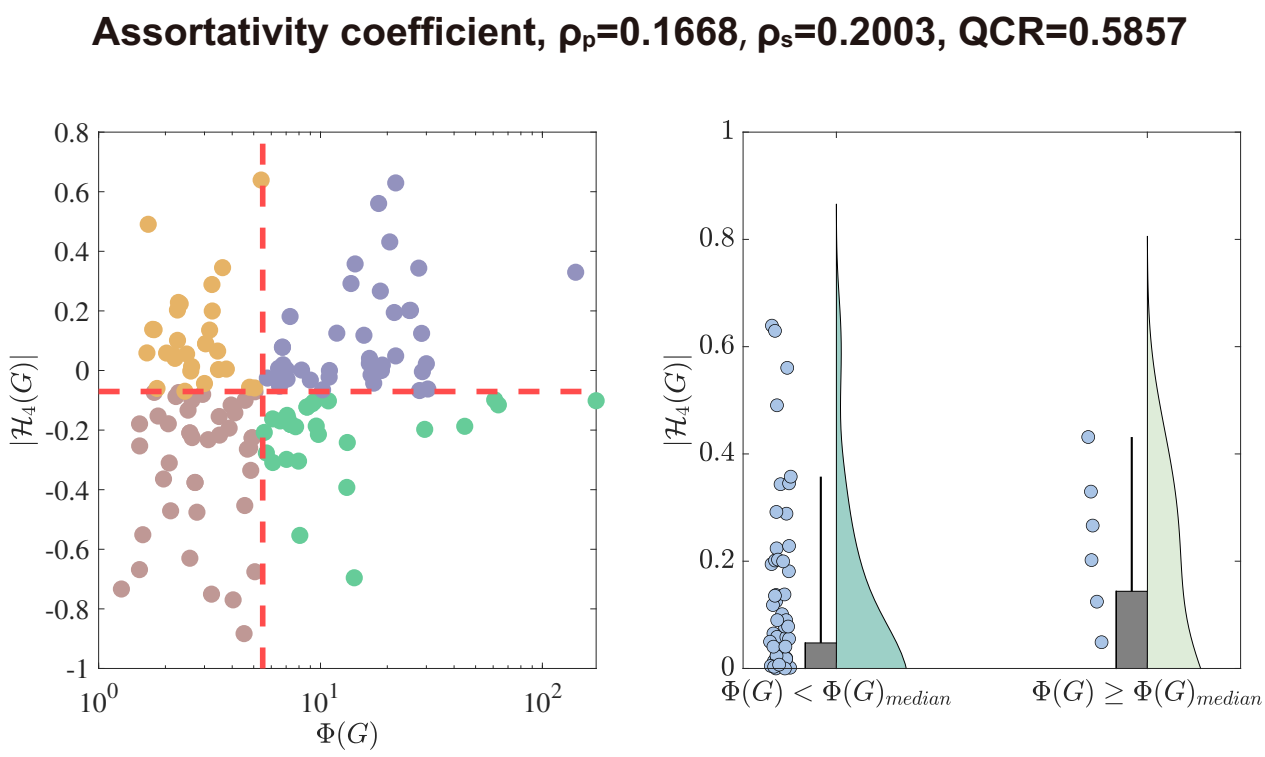

Fig. S19. Correlation between path multiplicity and assortativity coefficient in 140 real-world networks. The metadata and results for all 140 networks are given in Supplementary Materials. **a,** The left part of each panel presents a scatter plot along with the Pearson correlation ρ between $\Phi(G)$ and r. Each scatter plot is divided into four quadrants by the median values of $\Phi(G)$ and r and the Quadrant Count Ratio (QCR) is also shown. The right-hand violin plots show the distribution, mean and median values of the corresponding r, which are divided into two parts based on the median value of PMI. If there are more overlap between two violin subplots, it suggests a weaker correlation between the corresponding network metric and PMI.

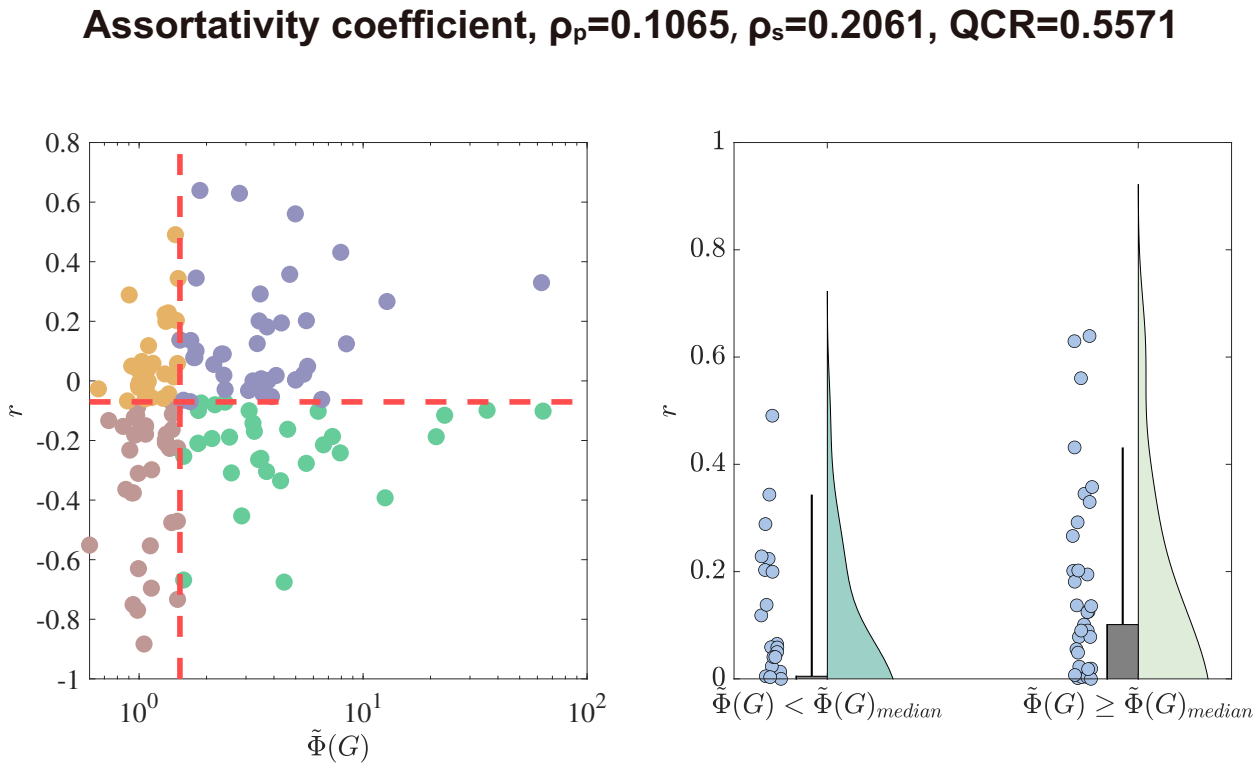

Fig. S20. Correlation between relative path multiplicity and assortativity coefficient in 140 real-world networks. The metadata and results for all 140 networks are given in Supplementary Materials. **a,** The left part of each panel presents a scatter plot along with the Pearson correlation ρ between $\tilde{\Phi}(G)$ and r. Each scatter plot is divided into four quadrants by the median values of $\tilde{\Phi}(G)$ and r and the Quadrant Count Ratio (QCR) is also shown. The right-hand violin plots show the distribution, mean and median values of the corresponding r, which are divided into two parts based on the median value of RPMI. If there are more overlap between two violin subplots, it suggests a weaker correlation between the corresponding network metric and RPMI.

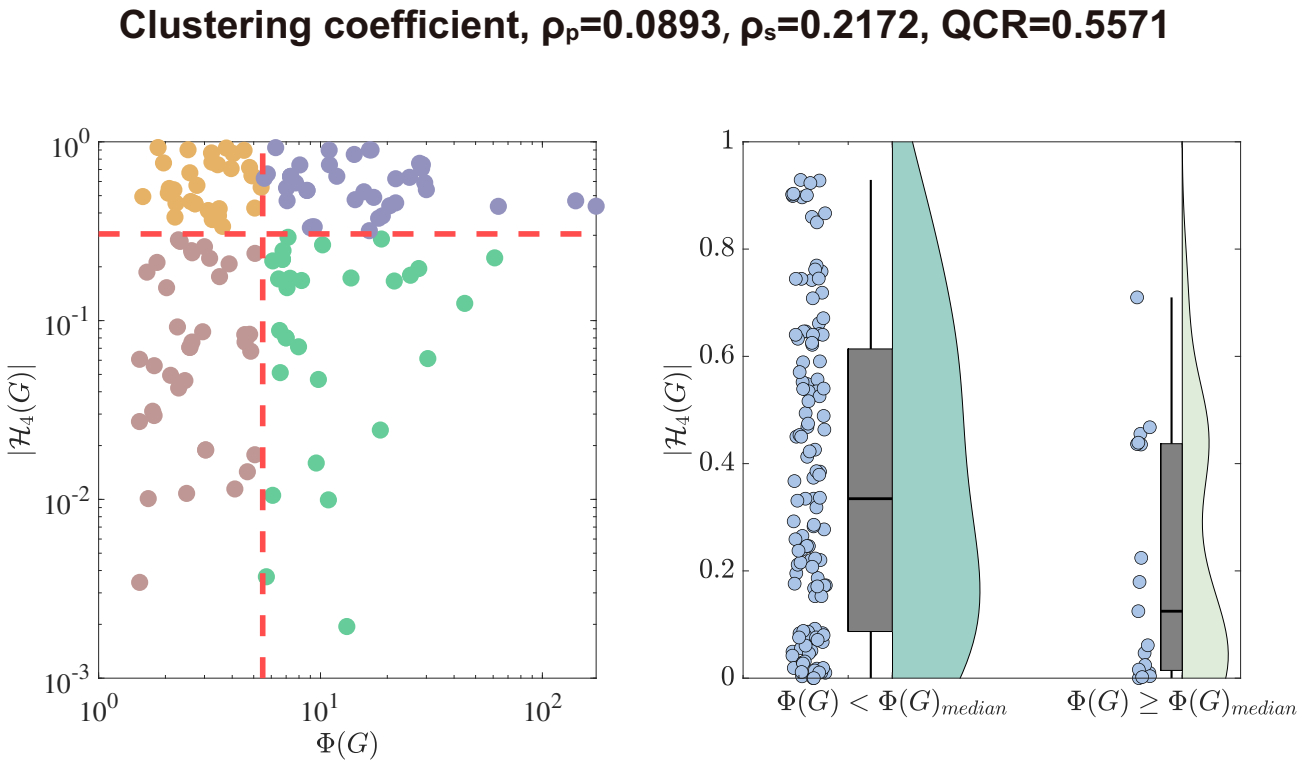

Fig. S21. Correlation between path multiplicity and clustering coefficient in 140 real-world networks. The metadata and results for all 140 networks are given in Supplementary Materials. **a,** The left part of each panel presents a scatter plot along with the Pearson correlation ρ between $\Phi(G)$ and C. Each scatter plot is divided into four quadrants by the median values of $\Phi(G)$ and C and the Quadrant Count Ratio (QCR) is also shown. The right-hand violin plots show the distribution, mean and median values of the corresponding C, which are divided into two parts based on the median value of PMI. If there are more overlap between two violin subplots, it suggests a weaker correlation between the corresponding network metric and PMI.

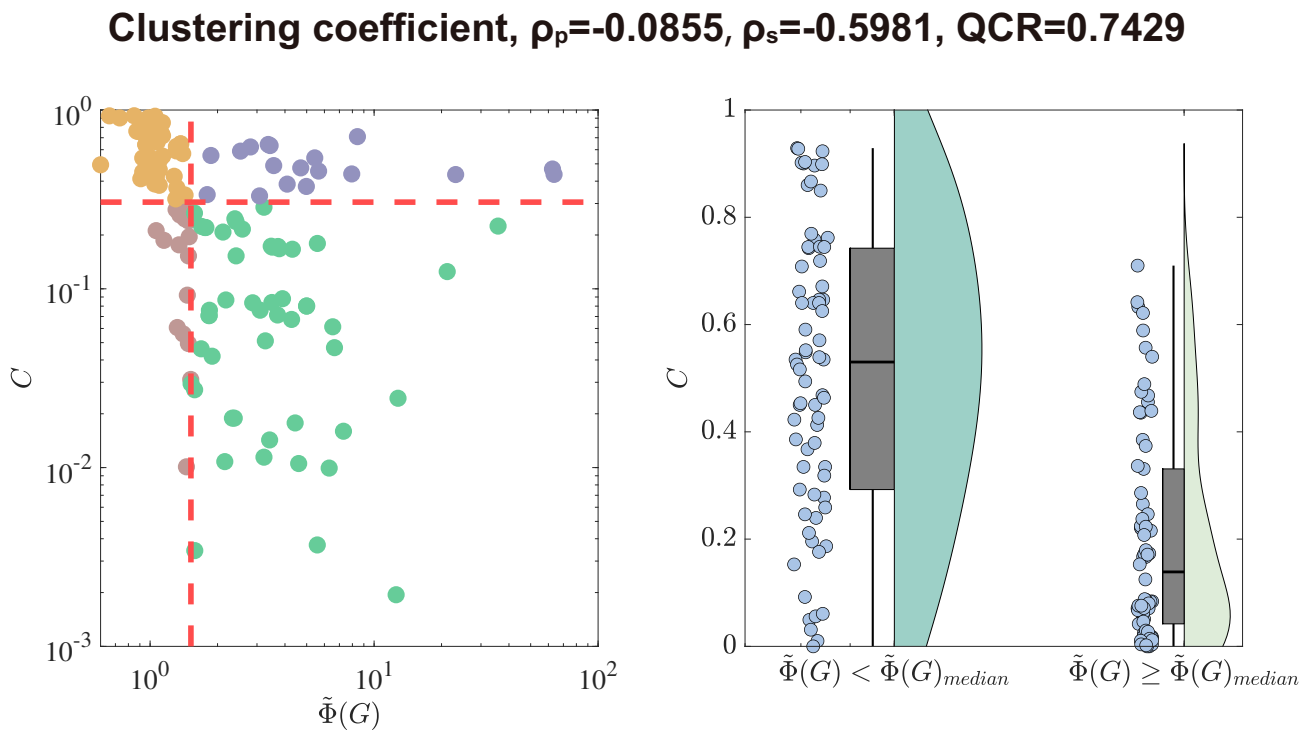

Fig. S22. Correlation between relative path multiplicity and clustering coefficient in 140 real-world networks. The metadata and results for all 140 networks are given in Supplementary Materials. **a,** The left part of each panel presents a scatter plot along with the Pearson correlation ρ between $\tilde{\Phi}(G)$ and C. Each scatter plot is divided into four quadrants by the median values of $\tilde{\Phi}(G)$ and C and the Quadrant Count Ratio (QCR) is also shown. The right-hand violin plots show the distribution, mean and median values of the corresponding C, which are divided into two parts based on the median value of RPMI. If there are more overlap between two violin subplots, it suggests a weaker correlation between the corresponding network metric and RPMI.

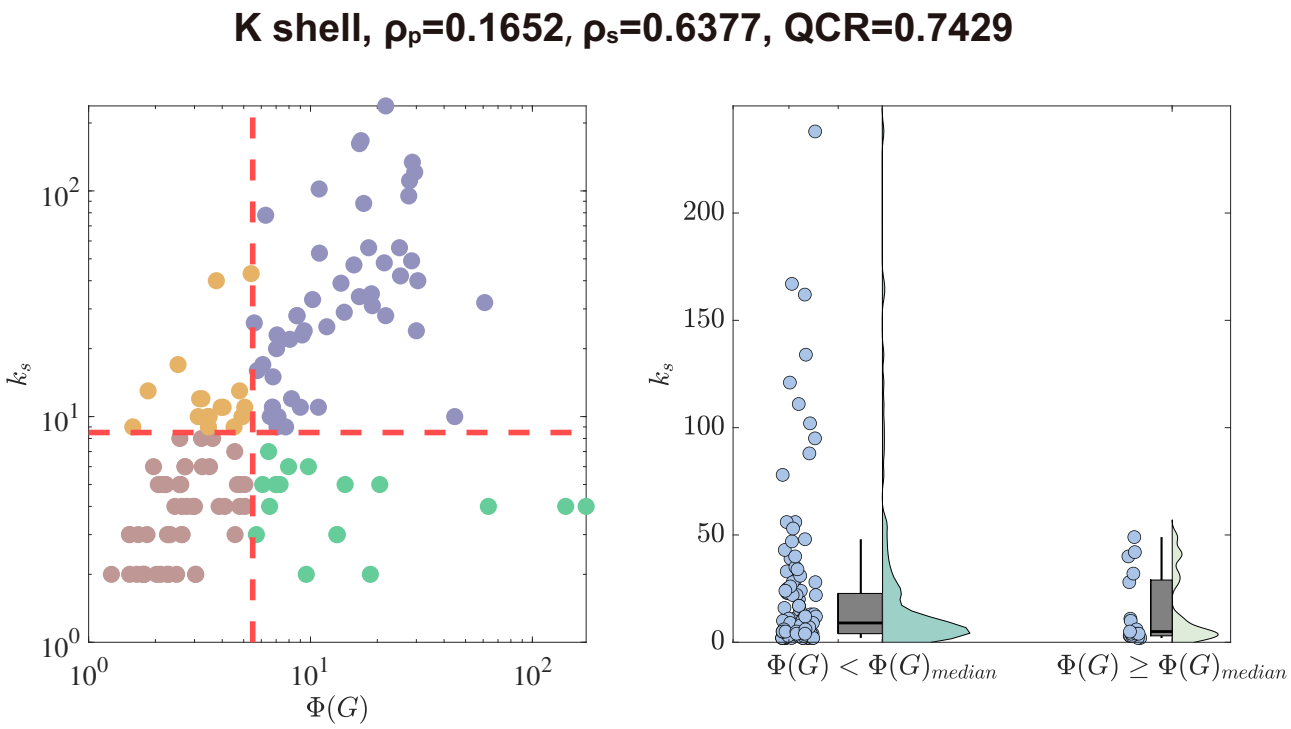

Fig. S23. Correlation between path multiplicity and K shell in 140 real-world networks. The metadata and results for all 140 networks are given in Supplementary Materials. **a,** The left part of each panel presents a scatter plot along with the Pearson correlation ρ between $\Phi(G)$ and k_s. Each scatter plot is divided into four quadrants by the median values of $\Phi(G)$ and k_s and the Quadrant Count Ratio (QCR) is also shown. The right-hand violin plots show the distribution, mean and median values of the corresponding k_s, which are divided into two parts based on the median value of PMI. If there are more overlap between two violin subplots, it suggests a weaker correlation between the corresponding network metric and PMI.

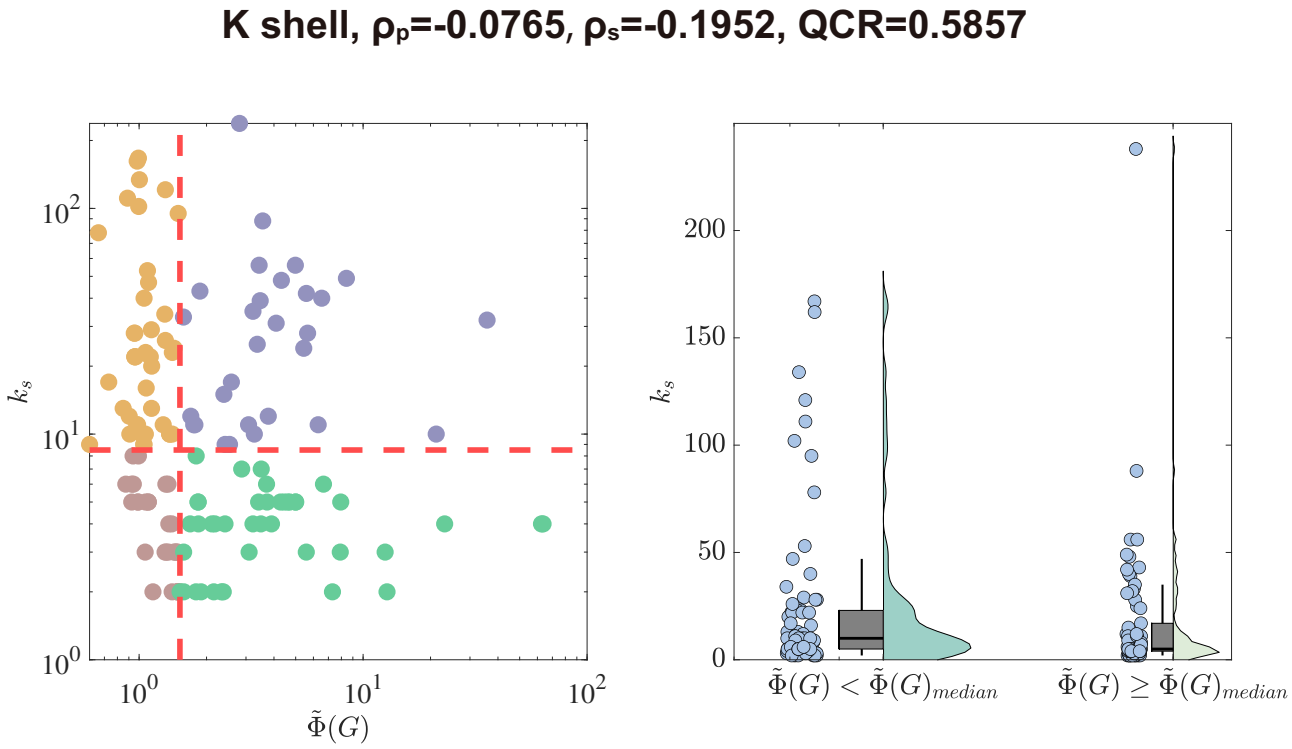

Fig. S24. Correlation between relative path multiplicity and K shell in 140 real-world networks. The metadata and results for all 140 networks are given in Supplementary Materials. **a,** The left part of each panel presents a scatter plot along with the Pearson correlation ρ between $\tilde{\Phi}(G)$ and k_s. Each scatter plot is divided into four quadrants by the median values of $\tilde{\Phi}(G)$ and k_s and the Quadrant Count Ratio (QCR) is also shown. The right-hand violin plots show the distribution, mean and median values of the corresponding k_s, which are divided into two parts based on the median value of RPMI. If there are more overlap between two violin subplots, it suggests a weaker correlation between the corresponding network metric and RPMI.

Ye Deng[1,2], Jun Wu[1,2,*], Xin Lu[3*], Petter Holme[4,5*], Daqing Li[6,7*], Zengru Di[1,2,8], Guanrong Chen[9], Jürgen Kurths[10,11]